On the turbulence in a magnetized plasma and its influence on the magnetoacoustic resonance

Autor(en): **Ritz, Ch.P. / Hoegger, B.A. / Sayasov, Y.S.**

Objekttyp: **Article**

Zeitschrift: **Helvetica Physica Acta**

Band (Jahr): **55 (1982)**

Heft 3

PDF erstellt am: **30.06.2024**

Persistenter Link: https://doi.org/10.5169/seals-115289

Helvetica Physica Acta, Vol. 55 (1982) 354–380 0018–0238/82/030354–27$1.50 + 0.20/0

On the turbulence in a magnetized plasma and its influence on the magnetoacoustic resonance[1])

By Ch. P. Ritz, B. A. Hoegger, Y. S. Sayasov, H. Schneider and B. G. Vaucher, Department of Physics, University of Fribourg, CH-1700 Fribourg/Switzerland

(13. III. 1982; rev. 10. V. 1982)

Abstract. The electrical conductivity of an inhomogeneous magnetized turbulent plasma for weak electromagnetic fields has been studied theoretically and experimentally. Our theory predicts a resistivity for radio frequency fields essentially controlled by the density fluctuations and the anisotropy of the turbulence. In order to determine these parameters the turbulent behaviour and driving mechanism have been examined. The theory is checked looking at the magnetoacoustic resonance behaviour which is very sensitive to the conductivity of the plasma.

The plasma was produced by microwave discharges. The plasma parameters are: mean electron density $\langle n_e \rangle = 1.5\ 10^{12}\,\mathrm{cm}^{-3}$, density gradient scale length $L_n = 0.6\,\mathrm{cm}$, mean electron temperature $\langle T_e \rangle = 2.5\,\mathrm{eV}$, magnetic field $B_0 = 2\,\mathrm{kGauss}$, neutral gas pressure $p_0 = 2.5\ 10^{-4}\,\mathrm{Torr}$ argon. The magnetoacoustic oscillations were excited using a long single turn coil as an antenna. The wave field profiles and the resonant amplification of the exciting magnetic field were measured. On the basis of the agreement between theory and experiments it is concluded that the anomalous damping of the magnetoacoustic oscillations can be explained mainly by the influence of drift-wave tubulence.

I. Introduction

One of the first experiments dealing with density fluctuations and modified diffusion across the magnetic field was reported by Bohm as early as 1949 [1]. Few years later Budden [2] showed that irregularities in the ionosphere may modify the refractive index of electromagnetic waves. In particular he gave a hint to explain the damping of whistlers by small density perturbations.

At the present time we have a considerable knowledge of a broad class of instabilities which arise by virtue of drifts in an inhomogeneous magnetized plasma. A comprehensive list of original literature can be found in Refs. [3–5]. Likewise we know that in a strongly unstable regime, drift-wave turbulence may develop through the non-linear interaction of drift instabilities [6, 7]. In consequence the transport coefficients (conductivity, diffusion coefficients) of the turbulent plasma in strong magnetic fields may differ greatly from those of a quiescent plasma, even for turbulences having a relatively small noise level.

[1]) Supported by the Swiss National Science Foundation.

An easy way to measure the electrical conductivity is to launch an electromagnetic wave into the plasma and to measure the geometric resonances [8, 9]. The first radial eigenmode can occur when approximately half a wave length coincides with the plasma diameter, provided the waves are not too strongly damped. Under such conditions the electromagnetic fields in the plasma can attain much larger amplitudes than at the boundary [10].

In contrast to experiments performed in fully ionized high density plasmas [11, 12], the plasmas of moderate density ($\langle n_e \rangle \simeq 10^{12}\,\mathrm{cm}^{-3}$, $\langle T_e \rangle \simeq 10 \cdot T_i = 2-8\,\mathrm{eV}$) show a much poorer resonance behaviour than expected from classical theory [13–16]. (The brackets $\langle\ \rangle$ denote mean values across the radial profile.) These latter experiments were characterized by strongly inhomogeneous radial density profiles. In the density gradient at the plasma edge, strong fluctuations were observed [15].

Therefore, we study in this article the unstable and turbulent behaviour of a strongly inhomogeneous plasma cylinder. Furthermore we study the influence of random density fluctuations on the electrical conductivity of the plasma and compare these results with our experiments.

In Section II we derive a conductivity tensor for a turbulent magnetoplasma which applies to electromagnetic r.f.-fields. The crucial aspect besides the radial profile of the random density fluctuations is the spatial anisotropy of the turbulence. In Section III we describe the experimental apparatus and measurement techniques. The digital spectral analysis, which enables us to explore the turbulence, is given special consideration. In Section IV our experimental observations are presented. The density gradient driven drift waves are identified and the development of turbulence is discussed. From a knowledge of the characteristics of turbulent plasma, the anisotropy and the random fraction of the fluctuation are estimated. Furthermore the magnetoacoustic resonance is numerically calculated considering the derived conductivity tensor. The result is compared with the measured resonance behaviour. Section V presents our conclusion.

II. Theory

1. *Assumptions*

To study the effect of turbulence on the electrical conductivity we consider the electrons and ions as two cold fluids. The target plasma is supposed not to be affected by the applied r.f.-field. In addition the following assumptions and approximations can be made, based on experimentally determined plasma parameters:

(1) The electrons are magnetized by the influence of a constant magnetic field $\mathbf{B}_0$ in the z-direction: $\nu_e \ll \omega_{c_e}$. ω_{c_e} is the electron cyclotron frequency and ν_e the total collision frequency of the electrons.
(2) The plasma is quasineutral: $n_e = n_i = n$.
(3) The mean electron density $\bar{n}(r)$ varies only in a radial direction. (The bar symbol denoting mean values across macroscopic space elements.)
(4) The mean quadratic density fluctuations are small $\overline{(n'/\bar{n})^2}(r) \ll 1$. $n'(r)$ is the random fluctuation around the mean density.

(5) The displacement current is negligible in the region of the first magnetoacoustic resonance frequency.
(6) The frequency of the density fluctuation ω_{fl} is much smaller than the frequency ω of the r.f.-field: $\omega_{fl} \ll \omega$. This allows the density variations to be considered as time independent thus requiring only the spacial fluctuations $n'(r)$ to be taken into account.
(7) The criteria $\omega_{c_i} \ll \omega \ll \omega_{c_e}$ and $\nu_{in} \ll \omega$ shall apply to the r.f.-field. ν_{in} is the collision frequency of the ions with neutral particles and ω_{c_i} is the ion cyclotron frequency.
(8) We consider small scale fluctuations characterized by an effective length l_{eff} that is small in comparision with field parameters as wavelength, skin-depth. This allows the fluctuating fields $\mathbf{E}'$ to be considered as being quasistatic.

2. *The electrical conductivity tensor for turbulent magnetized plasmas*

The fact that the plasma exhibits random density fluctuations can lead to a strong change in the electrical conductivity tensor compared with that of a quiescent plasma. This effect was investigated by Yoshikawa and Rose [18], Kadomtsev [19] and by Vedenov [20] for applied electrostatic fields. They considered a homogeneous magnetized plasma (with constant magnetic field $\mathbf{B}_0$ in z-direction) in agreement with our assumptions (1)–(5). In addition they superimposed a constant electric field $\mathbf{E}$ in the y-direction (Fig. 1) and neglected the ionic movement for the reasons explained in [19]. In the plasma without collisions the electrons describe a helical path in the x-direction as a result of the $\mathbf{E}\times\mathbf{B}_0$-drift. This is the Hall current $\mathbf{j}_d$. If the electrons collide with heavy particles this gives rise to a small current $\mathbf{j}_0$ parallel to the imposed field $\mathbf{E}$. Should the electron density also exhibit an additional random portion n' with $n(r) = \bar{n}(r) + n'(r)$ then, in addition to the undisturbed field $\mathbf{E}$, this will give rise to a fluctuating field $\mathbf{E}'$. The presence of the component $\mathbf{E}'$ leads to a drift of electrons in the y-direction. This turbulent current $\mathbf{j}'_d \propto \overline{n'E'}$ can be appreciably larger than the current $\mathbf{j}_0$ in the absence of density fluctuations.

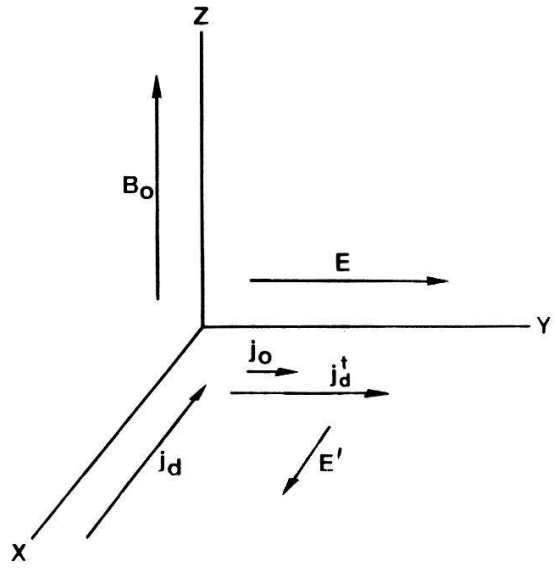

Figure 1
Schematic representation of the current in a magnetized plasma with and without density fluctuations. An external electric field $\mathbf{E}$ is applied parallel to the y-axis.

Intuitively it seems clear that this concept may be extended to r.f.-fields provided that the condition $\omega_{c_i} \ll \omega \ll \omega_{c_e}$ is fulfilled. In this case the electrons describe many loops within one period of the r.f.-field while the ions remain practically at rest. Thus the picture given in Fig. 1 should remain valid.

A detailed derivation of the conductivity tensor for r.f.-fields in turbulent magnetic plasma will be given now. The basic idea has been formulated in a simplified form in a previous letter [21].

Maxwell's equations and current density $\mathbf{j}$ are written in cgs-Gaussian units as:

$$\operatorname{rot}\mathbf{B}=\frac{4\pi}{c}\mathbf{j}, \qquad \operatorname{rot}\mathbf{E}=-\frac{1}{c}\frac{\partial\mathbf{B}}{\partial t}, \qquad \mathbf{j}=\mathbf{j}_e+\mathbf{j}_i. \tag{1}$$

Ohm's law becomes for electrons and ions respectively:

$$\begin{aligned} &\nu_e\mathbf{j}_e+\frac{\partial\mathbf{j}_e}{\partial t}=\frac{e^2n(r)}{m_e}\mathbf{E}-\omega_{c_e}[\mathbf{j}_e\times\mathbf{h}] \\ &\nu_i\mathbf{j}_i+\frac{\partial\mathbf{j}_i}{\partial t}=\frac{e^2n(r)}{m_i}\mathbf{E}, \qquad \omega_{c_e}=\frac{eB}{m_ec}, \qquad e>0 \end{aligned} \tag{2}$$

where $\mathbf{h}$ is the unit vector in the direction of the magnetic field $\mathbf{B}_0$. The equations (1) and (2) may be solved assuming the time dependent terms $\mathbf{E}, \mathbf{B}$ and $\mathbf{j}_\alpha$ ($\alpha = e, i$) to vary as $\exp(-i\omega t)$. Equation (2) gives

$$\begin{aligned} &(\nu_e-i\omega)\mathbf{j}_e=\frac{e^2}{m_e}(\bar{n}(r)+n'(r))\mathbf{E}-\omega_{c_e}[\mathbf{j}_e\times\mathbf{h}] \\ &(\nu_i-i\omega)\mathbf{j}_i=\frac{e^2}{m_i}(\bar{n}(r)+n'(r))\mathbf{E}. \end{aligned} \tag{3}$$

The values $\mathbf{E}, \mathbf{B}$ and $\mathbf{j}_\alpha$ are represented by the sum of the mean values across the macroscopic space elements $\bar{\mathbf{E}}, \bar{\mathbf{B}}, \bar{\mathbf{j}}_\alpha$ and that of their fluctuating components $\mathbf{E}', \mathbf{B}'$ and $\mathbf{j}'_\alpha$, that is $\mathbf{E}=\bar{\mathbf{E}}+\mathbf{E}', \mathbf{B}=\bar{\mathbf{B}}+\mathbf{B}', \mathbf{j}_\alpha=\bar{\mathbf{j}}_\alpha+\mathbf{j}'_\alpha$. This gives, from equation (1)

$$\operatorname{rot}\bar{\mathbf{E}}=i\frac{\omega}{c}\bar{\mathbf{B}}, \qquad \operatorname{rot}\bar{\mathbf{B}}=\frac{4\pi}{c}\bar{\mathbf{j}} \tag{4}$$

$$\operatorname{rot}\mathbf{E}'=i\frac{\omega}{c}\mathbf{B}', \qquad \operatorname{rot}\mathbf{B}'=\frac{4\pi}{c}\mathbf{j}' \quad \text{from which } \operatorname{div}\mathbf{j}'=0 \tag{5}$$

where

$$\bar{\mathbf{j}}=\bar{\mathbf{j}}_e+\bar{\mathbf{j}}_i, \qquad \mathbf{j}'=\mathbf{j}'_e+\mathbf{j}'_i. \tag{4a), (5a)}$$

The equations (3) can be split into equations for respective average magnitudes and random parts.

$$\bar{\mathbf{j}}_e=\sigma_{0_e}\bar{\mathbf{E}}+\overline{\mathbf{j}'_e}-\chi_e[\bar{\mathbf{j}}_e\times\mathbf{h}], \qquad \bar{\mathbf{j}}_i=\sigma_{0_i}\bar{\mathbf{E}} \tag{6a), (6b)}$$

$$\mathbf{j}'_e=\sigma_{0_e}\mathfrak{E}'+\mathbf{j}'^{t'}_e-\chi_e[\mathbf{j}'_e\times\mathbf{h}], \qquad \mathbf{j}'_i=\sigma_{0_i}\mathfrak{E}' \tag{7a), (7b)}$$

where

$$\chi_e=\frac{\omega_{ce}}{\nu_e-i\omega}, \qquad \sigma_{0_\alpha}=\frac{e^2\bar{n}}{m_\alpha(\nu_\alpha-i\omega)}, \qquad \mathfrak{E}'=\mathbf{E}'+\frac{n'}{\bar{n}}\bar{\mathbf{E}}$$

and

$$\mathbf{j}_e^t = \bar{\mathbf{j}}_e^t + \mathbf{j}_e^{t'} = \frac{e^2}{m_e(\nu_e - i\omega)}\, n'\mathbf{E}' = \frac{\sigma_{0_e}}{\bar{n}}\, n'\mathbf{E}' \tag{8}$$

The term $\mathbf{j}_e^t$ represents the turbulent current of the electrons. The term $\mathbf{j}_i^t = (\sigma_{0_i}/\bar{n})n'\mathbf{E}'$ representing the turbulent current of the ions is neglected as a result of assumption (7).

Expanding n' and $\mathbf{E}'$ into Fourier series

$$n' = \sum_{\mathbf{k}} n'_{\mathbf{k}}\, e^{i\mathbf{kr}}, \qquad \mathbf{E}' = \sum_{\mathbf{k}} \mathbf{E}'_{\mathbf{k}} e^{i\mathbf{kr}},$$

we can find an explicit form for $\bar{\mathbf{j}}_e^t$ and $\mathbf{j}_e^{t'}$, following the same procedure as Yoshikawa and Rose [18], equation (13, 14) of their paper. It follows that

$$\mathbf{j}_e^t = \frac{\sigma_{0_e}}{\bar{n}} \left[\sum_{\mathbf{k}_2} n'_{-\mathbf{k}_2} \mathbf{E}'_{\mathbf{k}_2} + \sum_{-\mathbf{k}_1 \neq \mathbf{k}_2} n'_{\mathbf{k}_1} \mathbf{E}'_{\mathbf{k}_2} e^{i(\mathbf{k}_1 + \mathbf{k}_2)\mathbf{r}} \right] \tag{9}$$

The first term in the bracket can be identified as the mean turbulent current

$$\bar{\mathbf{j}}_e^t = \frac{\sigma_{0_e}}{\bar{n}} \sum_{\mathbf{k}} n'^*_{\mathbf{k}} \mathbf{E}'_{\mathbf{k}} \tag{9a}$$

since $n'_{-\mathbf{k}} = n'^*_{\mathbf{k}}$ (n' is a real value). The second term in the bracket represents the random component $\mathbf{j}_e^{t'}$ and will be neglected, since $(\mathbf{k}_1 + \mathbf{k}_2) \cdot \mathbf{r}$ may be regarded as being randomly distributed (random phase approximation [22, 23]). This assumption is the basis of the theories of Yoshikawa, Rose [18], Kadomtsev [19] and also of this paper.

In the next section a relationship between $n'_{\mathbf{k}}$ and $\mathbf{E}'_{\mathbf{k}}$ is derived from (7a) governing the random current component $\mathbf{j}'_e$. From (7a) it follows with $\chi_e \gg 1$ (assumptions (1), (7)) that

$$j'_{e_x} = \sigma_1 \mathfrak{E}'_x + \sigma_2 \mathfrak{E}'_y, \qquad j'_{e_y} = -\sigma_2 \mathfrak{E}'_x + \sigma_1 \mathfrak{E}'_y, \qquad j'_{e_z} = \sigma_{0_e} \mathfrak{E}'_z \tag{10}$$

where

$$\sigma_1 = \frac{\sigma_{0_e}}{\chi_e^2}, \qquad \sigma_2 = -\frac{\sigma_{0_e}}{\chi_e}.$$

We now substitute (10) and (7b) in the equation $\operatorname{div} \mathbf{j}' = \operatorname{div} (\mathbf{j}'_e + \mathbf{j}'_i) = 0$ and assume that the spacial derivatives of the mean values $\bar{\mathbf{E}}$, $\bar{n}$ are much smaller than those of the fluctuating components $\mathbf{E}'$ and n' (assumption 8). Thus we assume that $\operatorname{rot} \mathbf{E}' = 0$)(*) and represent $\mathbf{E}'$ by an electrostatic potential ϕ'. We

*) Representing $\mathbf{E}'$ in the form $\mathbf{E}' = -\nabla\phi' + \delta\mathbf{E}'$ and treating $\delta\mathbf{E}'$ as a small perturbation, then $\delta\mathbf{E}'$ becomes negligible if the correlation length $l_{\mathbf{k}}$ of the density fluctuations $n'_{\mathbf{k}}$ is small compared with the characteristic magnitude of skin depth δ and wave length of the $\bar{\mathbf{E}}$ field λ: in short if $l_{\mathbf{k}} < \delta, \lambda$.

obtain the following expression:

$$(\sigma_1+\sigma_{0_i})\left(-\Delta_\perp\phi'+\frac{\partial n'}{\partial x}\frac{\bar{E}_x}{\bar{n}}+\frac{\partial n'}{\partial y}\frac{\bar{E}_y}{\bar{n}}\right)$$
$$+\sigma_2\left(\frac{\partial n'}{\partial x}\frac{\bar{E}_y}{\bar{n}}-\frac{\partial n'}{\partial y}\frac{\bar{E}_x}{\bar{n}}\right)+(\sigma_{0_e}+\sigma_{0_i})\left(-\frac{\partial^2\phi'}{\partial z^2}+\frac{\partial n'}{\partial z}\frac{\bar{E}_z}{\bar{n}}\right)=0. \tag{11}$$

($\Delta_\perp$ stands for the Laplace operator applied to the coordinates x and y). By Fourier analysis of n' and $\phi'=\sum_{\mathbf{k}}\phi'_{\mathbf{k}}e^{i\mathbf{kr}}$ the relationship between $\phi'_{\mathbf{k}}$ and $n'_{\mathbf{k}}$ is achieved:

$$\phi'_{\mathbf{k}}=i\frac{\chi_1(\bar{E}_x k_y-\bar{E}_y k_x)-\chi_2 k_z\bar{E}_z}{k_\perp^2+\chi_2 k_z^2}\frac{n'_{\mathbf{k}}}{\bar{n}} \tag{12}$$

where

$$\chi_1=\frac{\sigma_2}{\sigma_1+\sigma_{0_i}}=-\frac{\chi_e}{1+\chi_e^2\dfrac{m_e}{m_i}\dfrac{\nu_e-i\omega}{\nu_i-i\omega}}$$

$$\chi_2=\frac{\sigma_{0_e}}{\sigma_1+\sigma_{0_i}}=\frac{\chi_e^2}{1+\chi_e^2\dfrac{m_e}{m_i}\dfrac{\nu_e-i\omega}{\nu_i-i\omega}},\qquad k_\perp^2=k_x^2+k_y^2.$$

In equation (12) and in the following, terms of the order $1/\chi_1$ are neglected. The turbulent current $\mathbf{j}_e^t=-i\frac{\sigma_{0_e}}{\bar{n}}\sum_{\mathbf{k}}\mathbf{k}n'^*_{\mathbf{k}}\phi'_{\mathbf{k}}$ (9a) may now be split into the components

$$j_{e_x}^t=\sigma_{0_e}\sum_{\mathbf{k}}\left(\frac{n'_{\mathbf{k}}}{\bar{n}}\right)^2\frac{\chi_1(k_xk_y\bar{E}_x-k_x^2\bar{E}_y)-\chi_2k_xk_z\bar{E}_z}{k_\perp^2+\chi_2k_z^2}$$

$$j_{e_y}^t=\sigma_{0_e}\sum_{\mathbf{k}}\left(\frac{n'_{\mathbf{k}}}{\bar{n}}\right)^2\frac{\chi_1(k_y^2\bar{E}_x-k_xk_y\bar{E}_y)-\chi_2k_yk_z\bar{E}_z}{k_\perp^2+\chi_2k_z^2} \tag{13}$$

$$j_{e_z}^t=\sigma_{0_e}\sum_{\mathbf{k}}\left(\frac{n'_{\mathbf{k}}}{\bar{n}}\right)^2\frac{\chi_1(k_yk_z\bar{E}_x-k_xk_z\bar{E}_y)-\chi_2k_z^2\bar{E}_z}{k_\perp^2+\chi_2k_z^2}.$$

We replace now the sum over the wave vector $\mathbf{k}$ with the integral and define $\mathbf{k}$ in spherical coordinates (Fig. 2) using the relationships $k_z=k\cos\theta$, $k_x=k\sin\theta\cos\varphi$, $k_y=k\sin\theta\sin\varphi$ and $d\mathbf{k}=k^2\,d\cos\theta\,d\varphi\,dk$. We further define the mean random density fluctuations

$$\left(\frac{\Delta n}{\bar{n}}\right)^2=\left(\frac{n'}{\bar{n}}\right)^2=\int\left(\frac{n'_{\mathbf{k}}}{\bar{n}}\right)^2d\mathbf{k}=\int\left(\frac{n'_{\mathbf{k}}}{\bar{n}}\right)^2k^2\,dk\,d\varphi\,d\cos\theta \tag{14a}$$

and the angular distribution of the turbulent density fluctuations

$$R(\theta,\varphi)=\frac{\int\left(\dfrac{n'_{\mathbf{k}}}{\bar{n}}\right)^2k^2\,dk}{\left(\dfrac{\Delta n}{\bar{n}}\right)^2}=\frac{\Delta n^2(\theta,\varphi)}{\Delta n^2} \tag{14b}$$

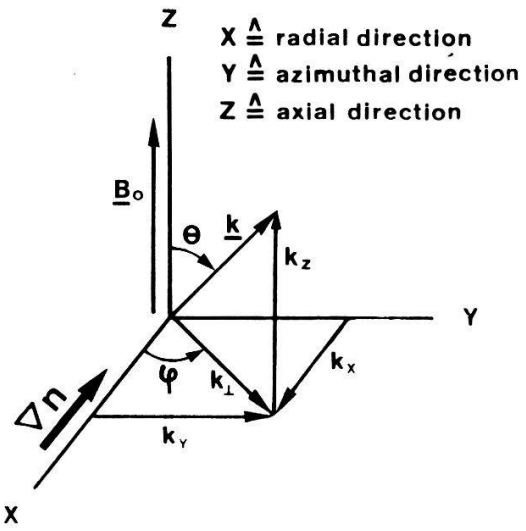

Figure 2
Definition of the component of the wave vector **k** in spherical coordinates.

where

$$\int_0^{\pi}\int_0^{2\pi} R(\theta,\varphi)\,d\varphi\,d\cos\theta = 1.$$

The factor $R(\theta,\varphi)$ consequently gives the fraction of the component $\Delta n^2(\theta,\varphi)$ having the wave vector in the direction (θ,φ) to the total random fluctuation Δn^2 and may be regarded as a measure of the spatial anisotropy of the turbulence.

The angular distribution of the density fluctuation is independent of the sign of the magnetic field direction $\mathbf{B}_0$ and is thus symmetric to the surface perpendicular to $\mathbf{B}_0$. Hence $R(\theta,\varphi) = R(\pi/2-\theta,\varphi)$. This condition leads to the disappearance of the terms containing the factors $k_x k_z$ and $k_y k_z$.

We may thus write the equations (13) in a simplified form

$$\begin{aligned}
j^t_{e_x} &= \sigma_{0_e}\left(\frac{\Delta n}{\bar n}\right)^2 \int_0^{\pi} d\cos\theta \int_0^{2\pi} d\varphi R(\theta,\varphi) \\
&\qquad \times \frac{\chi_1(\sin\varphi\cos\varphi\bar E_x - \cos^2\varphi\bar E_y)\sin^2\theta}{1+\chi_2\cos^2\theta} \\
j^t_{e_y} &= \sigma_{0_e}\left(\frac{\Delta n}{\bar n}\right)^2 \int_0^{\pi} d\cos\theta \int_0^{2\pi} d\varphi R(\theta,\varphi) \\
&\qquad \times \frac{\chi_1(\sin^2\varphi\bar E_x - \cos\varphi\sin\varphi\bar E_y)\sin^2\theta}{1+\chi_2\cos^2\theta} \qquad (15) \\
j^t_{e_z} &= \sigma_{0_e}\left(\frac{\Delta n}{\bar n}\right)^2 \int_0^{\pi} d\cos\theta \int_0^{2\pi} d\varphi R(\theta,\varphi)\,\frac{\chi_2\cos^2\theta\bar E_z}{1+\chi_2\cos^2\theta}.
\end{aligned}$$

The term $1/(1+\chi_2\cos^2\theta)$ in equation (15) behaves as a δ-function peaking at $\pi/2$ and vanishing outside the angular region $\Delta\theta = |\pi/2-\theta| \ll 1/|\chi_2| \ll 1$. If the spatial anisotropy of the turbulent eddies varies only slightly in the angular region $\Delta\theta$, we

may set $R(\theta, \varphi) = R(\pi/2, \varphi)$. Integrating (15) yields

$$j^t_{e_x} = \pm\sigma_{0_e}\left(\frac{\Delta n}{\bar{n}}\right)^2 \pi\left(\int_0^{2\pi} R(\pi/2, \varphi)\sin\varphi\cos\varphi\, d\varphi \bar{E}_x - \int_0^{2\pi} R(\pi/2, \varphi)\cos^2\varphi\, d\varphi \bar{E}_y\right)\frac{\chi_1}{\sqrt{\chi_2}}$$

$$j^t_{e_y} = \pm\sigma_{0_e}\left(\frac{\Delta n}{\bar{n}}\right)^2 \pi\left(\int_0^{2\pi} R(\pi/2, \varphi)\sin^2\varphi\, d\varphi \bar{E}_x - \int_0^{2\pi} R(\pi/2, \varphi)\sin\varphi\cos\varphi\, d\varphi \bar{E}_y\right)\frac{\chi_1}{\sqrt{\chi_2}} \quad (16)$$

$$j^t_{e_z} = -\sigma_{0_e}\left(\frac{\Delta n}{\bar{n}}\right)^2 \bar{E}_z.$$

It can be shown that for the assumed conditions always the plus sign applies.

Substituting $\mathbf{j}^t_e$ (equation (16)) in the equation for the mean current $\bar{\mathbf{j}}_e$ (equation (6a)) and neglecting terms of order $(\Delta n/\bar{n})^2 \cdot |\sqrt{\chi_2}|$ against $|\chi_e|$ the conductivity tensor $\boldsymbol{\sigma}_e$ is found. (In the following the bar sign indicating mean values will be omitted.)

$$\boldsymbol{\sigma}_e = \begin{pmatrix} \sigma_{xx} & -\sigma_{xy} & 0 \\ \sigma_{xy} & \sigma_{yy} & 0 \\ 0 & 0 & \sigma_{zz} \end{pmatrix} \quad \text{with} \quad \sigma_{xx} = \frac{\sigma_{0_e}}{\chi_e^2} A_x, \quad \sigma_{yy} = \frac{\sigma_{0_e}}{\chi_e^2} A_y, \quad \sigma_{xy} = \frac{\sigma_{0_e}}{\chi_e}, \quad \sigma_{zz} = \sigma_{0_e} \quad (17)$$

and

$$A_x = 1 + \frac{\pi\left(\frac{\Delta n}{\bar{n}}\right)^2 \chi_e}{\sqrt{1 + \chi_e^2 \frac{m_e}{m_i}\frac{\nu_e - i\omega}{\nu_i - i\omega}}} \int_0^{2\pi} R\left(\frac{\pi}{2}, \varphi\right)\sin^2\varphi\, d\varphi$$

$$A_y = 1 + \frac{\pi\left(\frac{\Delta n}{\bar{n}}\right)^2 \chi_e}{\sqrt{1 + \chi_e^2 \frac{m_e}{m_i}\frac{\nu_e - i\omega}{\nu_i - i\omega}}} \int_0^{2\pi} R\left(\frac{\pi}{2}, \varphi\right)\cos^2\varphi\, d\varphi.$$

The total current $\mathbf{j}$ is as a result of the equations (4a) and (6) given by Ohms law

$$\mathbf{j} = \boldsymbol{\sigma}\mathbf{E} = (\boldsymbol{\sigma}_e + \sigma_{0_i} \cdot \mathbf{1})\mathbf{E} \quad \text{with} \quad \boldsymbol{\sigma} = \boldsymbol{\sigma}_e + \sigma_{0_i} \cdot \mathbf{1} \quad (18)$$

whereby $\boldsymbol{\sigma}_e$ is defined by equation (17) and where $\mathbf{1}$ represents the unit tensor. As can be seen from (17), the turbulence substantially increase the current of electrons perpendicular to $\mathbf{B}_0$, since $\sigma_{xx}, \sigma_{yy} \propto (\nu_e - i\omega)A_{x,y}$, with $|A| \simeq 100$ in our experiment.

If the fluctuations in $k_\perp$ are isotropic ($R(\pi/2, \varphi) = \text{const.}$), then as a result of equation (15):

$$A_x = A_y = 1 + \frac{\pi\left(\frac{\Delta n}{\bar{n}}\right)^2 \chi_e}{4\sqrt{1+\chi_e^2 \frac{m_e}{m_i}\frac{\nu_e - i\omega}{\nu_i - i\omega}}} J \tag{19}$$

with $J = 4\pi R(\theta = \pi/2)$.
If the tubulence is isotropic in all directions, we have $J = 1$.

III. Apparatus and methods of measurement

1. *Apparatus, plasma production, analog signal processing*

The plasma is produced in a glass cylinder with inner radius of 4.6 cm and 120 cm length. A stationary magnetic field of 2 kGauss is produced in a solenoid consisting of 20 water cooled coils. The inhomogeneity in the field is less than 1%. For the pre-ionization with microwaves (2.45 GHz) the magnetic field on one side of the cylinder is locally reduced to 880 Gauss to achieve the electron cyclotron resonance. The main ionization results from two further slow wave structures (Fig. 3) by nonlinear absorption of the microwave power at about 0.5 ω_{c_e} [24]. The plasma is produced in pulses with a repetition rate of 50 Hz and pulse length of 3–4 ms.

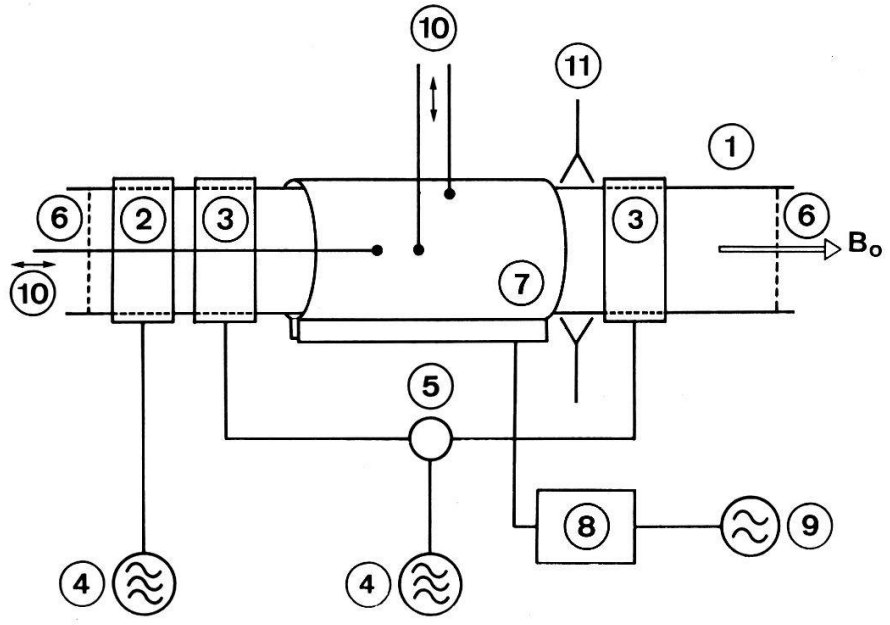

Figure 3
Sketch of the experimental apparatus. (1) discharge tube, (2) slow wave structure for preionization, (3) slow wave structure for plasma production, (4) microwave generator, (5) hybrid ring, (6) grid, (7) single turn coil, (8) impedance matching circuit, (9) r.f. amplifier and function generator, (10) probes, (11) 8 mm interferometer.

Magnetoacoustic waves are excited in a along single turn coil around the plasma cylinder (7 in Fig. 3). The coil can be matched to the impedance of the r.f.-generator within a frequency band of 3–30 MHz with a standing wave ratio better than 1.2. The pulse length of the r.f. can be varied and triggered at will. The field distribution of the excited r.f.-field is measured using a magnetic field probe, which can be displaced in the plasma in both radial and axial direction. The signals of this magnetic probe (B_z-component) can be observed during the period of plasma production as well as at the beginning of the afterglow. There is no difference in the amplification. Of course the signal of these waves during plasma production is somewhat noisy and the determination of the phase shift is much more reliable in the afterglow. The period of observation ($\lesssim 10\ \mu$s) is so short, that the plasma can be regarded as constant in time. Further the r.f.-power was limited to smaller values than 0.2 watt PEP (peak envelope power) to avoid nonlinear effects [25].

The mean electron density $\langle n_e(r)\rangle$ is determined using an 8 mm microwave interferometer. The radial and axial density profiles are obtained from measurements made with cylindrical Langmuir probes and double probes.

The temperature of the electrons is also determined using independent measuring techniques, as well as from Langmuir and double probe signals as from the sound velocity of the ion acoustic test waves. The diamagnetic probe gives a slightly higher electron temperature than the other measurements.

A more detailed description of the device as well as of the measurement technique is given in [15].

Measurement of the density fluctuations. To measure the density fluctuations we use cylindrical Langmuir probes and double probes which are operated in the ion saturation current. The probe tips are made of tungsten (2 mm long and 0.1 mm in diameter) and are arranged parallel to the magnetic field. Particular attention was given to the cleaning of the surface of the probe in order to minimize the effects of induced fluctuation.

The frequency response of the single probes were checked in a test arrangement identical to that of Roth and Krawczonek [26]. It was found that the response of the probes can be taken to be constant within the region of interest (below about 1 MHz). This of course is not true for higher frequencies as was shown by different authors [26, 27]. The resulting spectra, measured in the plasma, were identical for single probes, double probes and capacitive probes. We therefore conclude that the results are reliable and we are not misled by the self induced noise and frequency response.

The signal from the probes are digitized in a transient recorder (Biomation 8100) with two channels each having an $N = 1024$ word memory capacity and 8 bit amplitude resolution. The data are then stored on disc for processing in a minicomputer (type PDP 11/34). Figure 4 shows the schematic setup.

Particular care must be given to the frequency spectrum of the signal prior to digitizing: The maximum resolvable frequency (the Nyquist frequency $f_{\mathrm{Nyq}} = 1/(2\Delta t)$) of the digital time series is determined by the sampling interval Δt between two adjacent points of measurement. Frequencies above the Nyquist frequency gives rise to low frequency components in the spectrum. This effect known as aliasing [e.g. 28] may be avoided by filtering the signal prior to digitizing. To do this we use two identical band pass filters of the type Krohn–Hite 3103 (−24 dB/octave).

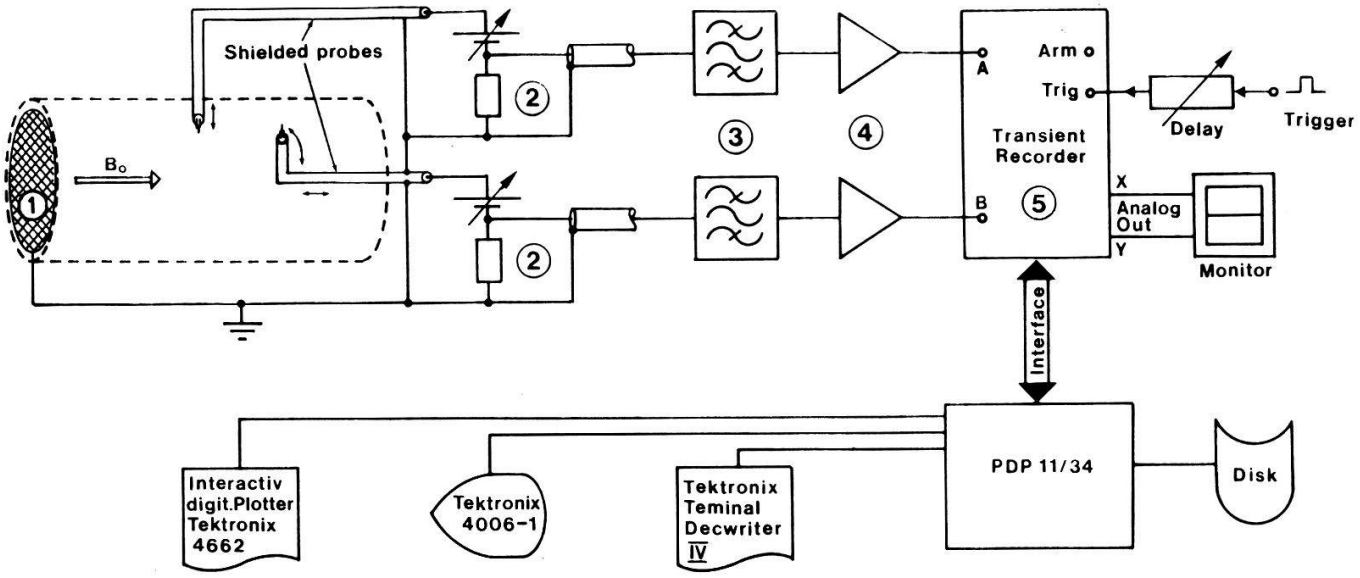

Figure 4
Schematic setup for the digital spectral analysis. (1) grid (reference for the single probe measurement), (2) identical movable probes with electrical circuits (can be replaced by double probes and capacitive probes), (3) Krohn-Hite band pass filters, (4) c.r.t.-amplifiers, (5) transient recorder, connected by an interface to the PDP 11/34 and peripherals.

The record length $T = N \cdot \Delta t$ must be long enough to allow a good frequency resolution $\Delta f_{\text{res}} = 1/T$ (in our experiment $\leqslant 1$ kHz). We thus measure during typically 2 ms and this is only possible during plasma production. But to avoid the initial-phase transients and to be in a quasi steady-state regime of the fluctuations, an appropriate time delay was used.

In order to utilize the full dynamic capability of the transient recorder for resolving the fluctuation, we filter out the low frequency components ($\leqslant 3$ kHz) due to the slowly changing mean density. Figure 5 shows typical digitized signals obtained from two spacially separated single probes operating in the ion saturation current.

2. *Digitial spectral analysis*

Once the fluctuations are measured these time series must be analyzed. A mathematical and statistical method is applied to give the wanted information, namely the frequency spectra, the dispersion relation of the fluctuation, the coherence and an eventual anisotropy of the turbulence. Also the coupling of different spectral components may be investigated by means of spectral analysis. These methods are well known and can be found in different books and articles [e.g. 29–32].

In general the evaluation of the space–time relationship of the fluctuation in a system requires correlation measurements across the entire volume. However, if the plasma fluctuation can be described by the superposition of an infinite set of monochromatic plane waves propagating in the direction of the corresponding wave vector, the problem is simplified essentially. Then the signal $\varphi_X(\mathbf{x}, t)$ from the probe X at the position $\mathbf{x}$ can be written

$$\varphi_X(\mathbf{x}, t) = \int_{-\infty}^{\infty} \phi_X(\omega) e^{i\mathbf{k}(\omega)\mathbf{x} - i\omega t}\, d\omega, \tag{20}$$

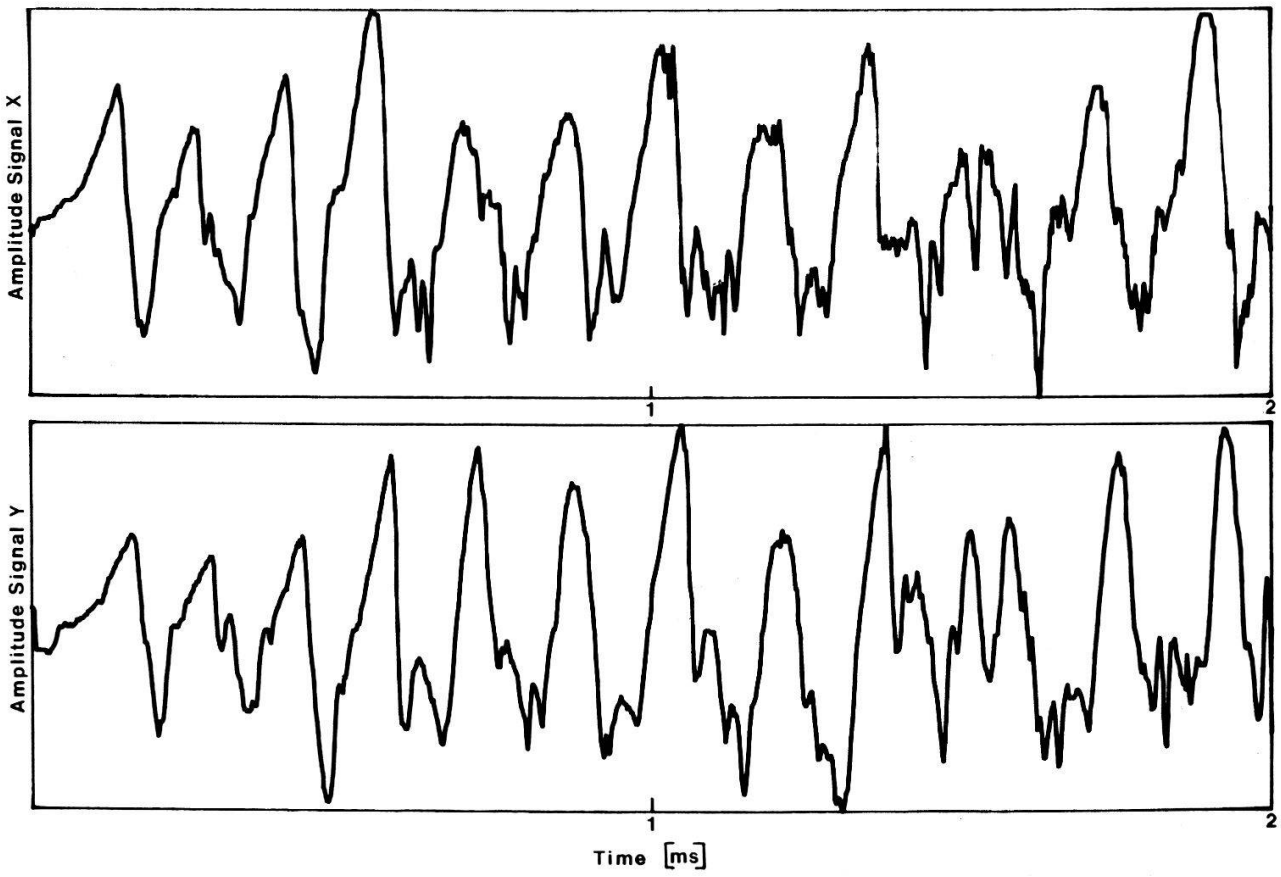

Figure 5
Typical digitized signals from two single probes X and Y operating in the ion saturation current. The probes are positioned to maximum density fluctuation and are azimuthally separated by 60 degrees. The small phase shift of the dominant mode ($m = 1$) due to the wave propagation between the two probes should be noted.

$\phi_X(\omega)$ representing the amplitude function and $\mathbf{k} = \mathbf{k}(\omega)$ being determined from the dispersion relation for linear modes.

The first step in the calculation consists in computing the Fourier transformation of $\varphi_X(\mathbf{x}, t)$. This gives

$$\Phi_X(\mathbf{x}, \omega) = \phi_X(\omega) e^{i\mathbf{k}(\omega)\mathbf{x}} = |\Phi_X(\mathbf{x}, \omega)|\, e^{i\theta_x(\mathbf{x},\omega)}. \tag{21}$$

If the fluctuations are measured with two different probes X and Y fixed at different points separated from one another by $\Delta\mathbf{x} = \mathbf{y} - \mathbf{x}$ then the *cross-power spectrum* $P_{XY}(\Delta\mathbf{x}, \omega)$(*) can be estimated from the corresponding Fourier spectra $\Phi_X(\mathbf{x}, \omega)$ and $\Phi_Y(\mathbf{y}, \omega)$

$$P_{XY}(\Delta\mathbf{x}, \omega) = \lim_{T\to\infty} \frac{1}{T} E[\Phi_X^*(\mathbf{x}, \omega) \cdot \Phi_Y(\mathbf{y}, \omega)]. \tag{22}$$

$E[\ ]$ represents the expected value and the asterisk stands for the complex conjugate. The cross-power spectrum gives the coherent power between two

*) Mathematically, the cross-power spectrum corresponds to a Fourier transform of the cross-correlation function

$$C_{XY}(\Delta\mathbf{x}, \tau) = \lim_{T\to\infty} \frac{1}{T} E[\varphi_X(\mathbf{x}, t) \cdot \varphi_Y(\mathbf{y}, t+\tau)].$$

probes. Since the cross-power spectrum is a complex function, it may be written (see equation (21))

$$P_{XY}(\Delta\mathbf{x}, \omega) = |P_{XY}(\Delta\mathbf{x}, \omega)|\, e^{i\theta_{XY}(\Delta\mathbf{x}, \omega)} = \lim_{T\to\infty} \frac{1}{T} E[|\Phi_X^* \Phi_Y|\, e^{i(\theta_y(\mathbf{y}, \omega) - \theta_x(\mathbf{x}, \omega))}]. \tag{23}$$

For fully incoherent signals the cross-power spectrum disappears, even though the product of the Fourier spectra from both probes is not equal to null. However since the phases are random, $P_{XY}(\Delta\mathbf{x}, \omega)$ will, when estimated over a large number of spectra, tend to null. The *phase spectrum* $\theta_{XY}(\Delta\mathbf{x}, \omega)$ represents the mean phase shift of the spectral components ω as the wave propagates the distance $\Delta\mathbf{x}$ between the probes. Thus the wave vector $\mathbf{k}(\omega)$ is given by

$$\theta_{XY}(\Delta\mathbf{x}, \omega) = \mathbf{k}(\omega) \cdot \Delta\mathbf{x}. \tag{24}$$

A special case of the cross-power spectrum is the *auto-power spectrum* $P_{XX}(\omega)$. Here both probes are considered to be at identical position. So there is only one probe signal and the auto-power spectrum gives the power as function of ω at this point.

The *coherence spectrum* coh_{XY} $(\Delta\mathbf{x}, \omega)$ can be defined as:

$$\mathrm{coh}_{XY}(\Delta\mathbf{x}, \omega) = \frac{|P_{XY}(\Delta\mathbf{x}, \omega)|}{[P_{XX}(\omega) P_{YY}(\omega)]^{1/2}}. \tag{25}$$

The coherence spectrum gives the ratio of the coherent power to the total power of the fluctuation between two probes as function of the frequency.

In the absence of any background noise the coherence of an undamped wave must be unity, independent of the probe separation. If there is a dissipation of energy, then the wave will be damped and the coherence decreases. The damping is connected with a frequency broadening as can be seen formally from the Fourier transformation of a wave with complex frequency ω_0. As a result the wave vector $\mathbf{k}$ for a definite frequency ω is no longer single valued (dispersion relation broadening).

In a turbulent medium the probe signals are incoherent when the probes are sufficiently separated from one another. If the probe separation becomes smaller than the characteristic dimension of the turbulent eddies at the respective frequency ω, then the coherence increases. The dependence of the coherence spectrum upon the probe separation can as a result be used to find the coherence length and if this is done in different directions the anisotropy of the turbulence can be estimated (see also [33] p. 341, p. 451, [27]).

Another question is, whether different spectral components in the plasma couple together or not. This problem is of general interest since new spectral components can be generated through nonlinear interaction between the modes. With the aid of higher-order spectra it is experimentally possible to distinguish between spontaneously excited modes and coupled modes. One thus obtains a physical insight into the generation-mechanism of the fluctuation.

For the analysis of three-wave coupling the bispectrum is sufficient [31]. In this case the frequencies and wave-numbers must satisfy the resonance condition $\omega_1 + \omega_2 = \omega_3$ and $k_1 + k_2 = k_3 + \Delta k$, where Δk is the wavenumber mismatch.

The *bispectrum* $B_X(\omega_1, \omega_2)$(*) may be defined [34] as

$$B_X(\omega_1, \omega_2) = \lim_{T\to\infty} \frac{1}{T} E[\Phi_X(\mathbf{x}, \omega_1) \cdot \Phi_X(\mathbf{x}, \omega_2) \cdot \Phi_X^*(\mathbf{x}, \omega_1+\omega_2)]. \tag{26}$$

The bispectrum allows spontaneously excited waves to be distinguished from coupled waves by measuring the phase coherence between the modes. Should the waves of a spectrum of frequency $\omega_1, \omega_2, \omega_1+\omega_2$ be independent then their Fourier transforms will also show random phase relationships (equation (21)). In calculating the expected value, the complex vectors average out (similar to equation (23)) and the bispectrum becomes null. However if the waves $\omega_1, \omega_2, \omega_1+\omega_2$ are coupled – as a result of nonlinear interaction – then the calculated Fourier components will exhibit a constant phase relationship

$$\Delta\theta(\omega_1, \omega_2) = \theta(\omega_1)+\theta(\omega_2)-\theta(\omega_1+\omega_2) \tag{26a}$$

to one another and the bispectrum will attain a finite value. $\Delta\theta$ is called *biphase spectrum* [35].

Most important for us is the *bicoherence spectrum* which may be defined analog to the coherence spectrum as

$$b^2(\omega_1, \omega_2) = \lim_{T\to\infty} \frac{1}{T} \frac{|B_X(\omega_1, \omega_2)|^2}{E[|\Phi_X(\mathbf{x}, \omega_1) \cdot \Phi_X(\mathbf{x}, \omega_2)|^2] \cdot E[|\Phi_X(\mathbf{x}, \omega_1+\omega_2)|^2]}. \tag{27}$$

$b^2(\omega_1, \omega_2)$ measures the fraction of the power at the frequency $\omega_3 = \omega_1+\omega_2$, which is connected to the waves of frequency ω_1 and ω_2 by three-wave coupling.

The bispectral analysis gives information about the stimulating mechanism which leads to the formation of a turbulent spectrum ([6, 35]).

Computing technique. The digitized time series $(x_k, k = 1, N)$ of an analog signal $(x(t), t = 1, T)$ is subsequently processed using the following procedure: Each time series is passed through a filter to eliminate the linear trend component $(x_k = a \cdot k \cdot \Delta t + b)$. a and b are estimated from the method of least square regression. A function known as a Hanning window [36]: $x_H(t) = \frac{1}{2}(1-\cos(2\pi t/T)) \cdot x(t)$ is used to reduce leakage caused by the finite record length of each time series. The Fourier transformation is carried out by FFT-technique. The desired spectrum is calculated according to the spectral analysis technique discussed above. The expected value is estimated by averaging across M independent data sets. The relative standard error δ of the estimate is [31]: coherence $\delta_{\text{coh}} \simeq \sqrt{(1-\text{coh}^2)/M}$ bicoherence $\delta_b \simeq \sqrt{(1-b^2)/M}$. The variance of the expected value is further reduced according to [37, 30] by frequency averaging (data smoothing).

---

*) Mathematically the bispectrum corresponds to a two-dimensional Fourier transform of a second-order correlation function

$$C_X(\tau_1, \tau_2) = \lim_{T\to\infty} \frac{1}{T} E[\varphi_X(\mathbf{x}, t) \cdot \varphi_X(\mathbf{x}, y+\tau_1) \cdot \varphi_X(x, t+\tau_2)].$$

IV. Experimental observations and discussion

In this section initially the plasma parameters are presented. Then we give the results of density fluctuation measurements which lead to the identification of the instability. We further examine the turbulence, its driving mechanism and the anisotropy. Thus all values entering into the conductivity tensor (Section II) are determined. Finally, the magnetoacoustic resonance, as measured in our experiment, is compared with the predictions of our theory.

The plasma parameters are determined using the experimental techniques described in Section III. The principal parameters are summarized in Table 1. Figure 6(a) shows the radial density and temperature profiles. The density is strongly inhomogeneous. Note the pronounced gradient in the edge zone. We further observe density fluctuations in our plasma (Fig. 5) which attains a maximum in the region of the greatest density gradient (Fig. 6(b)). The auto-power spectrum for this probe position is shown in Fig. 7(a). Two marked peaks at 6 kHz and 14 kHz appear in the broad band spectrum.

1. *Drift instability*

The appearance of strong density fluctuations in the density gradient suggest the idea of drift instabilities. In order to identify the type of instability we must know the direction of the wave propagation, its wave length and phase velocity.

The directional dependence of the fluctuation is measured with the help of the cross-power spectrum. Figure 8 represents a typical set of spectra from one such position whereby an average was made over 25 data sets. For this measurement both probes are positioned at the radius $r_{max} = 3.5$ cm. Here the fluctuations have their maximum. But azimuthally the probes are separated by $\Delta\phi = 60°$.

The phase shift θ_{XY} of the cross-power spectrum (equation (23)) for the very marked first peak at 6 kHz is shown in Fig. 9 for different azimuthal probe separations $\Delta\phi$. Because the phase shift is equal to the angle between the probes, the wave length λ_ϕ at this frequency is equal to $2 \cdot r_{max} \cdot \pi$. The azimuthal phase velocity is thus $v_\phi = 1.4\ 10^5$ cm/s.

In a next step we determine the component λ_z of this dominant wave. The

Table 1
Plasma parameters

Argon plasma			
electron temperature	$\langle T_e(r)\rangle = 2.5$ eV	collision frequencies:	$\nu_{en} = 1.4\ 10^6\ s^{-1}$
			$\langle \nu_{ei}(r)\rangle = 1.5\ 10^7\ s^{-1}$
ion temperature	$T_i = 0.3$ eV		$\nu_{in} = 1.1\ 10^4\ s^{-1}$
mean electron density	$\langle n_e(r)\rangle = 1.5\ 10^{12}\ cm^{-3}$	plasma length	$L_{pl} = 100$ cm
		radius	$R_{pl} = 4.6$ cm
density gradient scale length $(Vn/n)^{-1}$	$L = 0.6$ cm	excitation coil: length	$L_c = 40$ cm
		radius	$R_c = 5$ cm
neutral gas pressure	$p_0 = 0.25$ m Torr		
external magnetic field	$B_0 = 2$ kGauss		
cyclotron frequencies:	$\omega_{ce} = 3.4\ 10^{10}\ s^{-1}$		
	$\omega_{ci} = 4.6\ 10^5\ s^{-1}$		

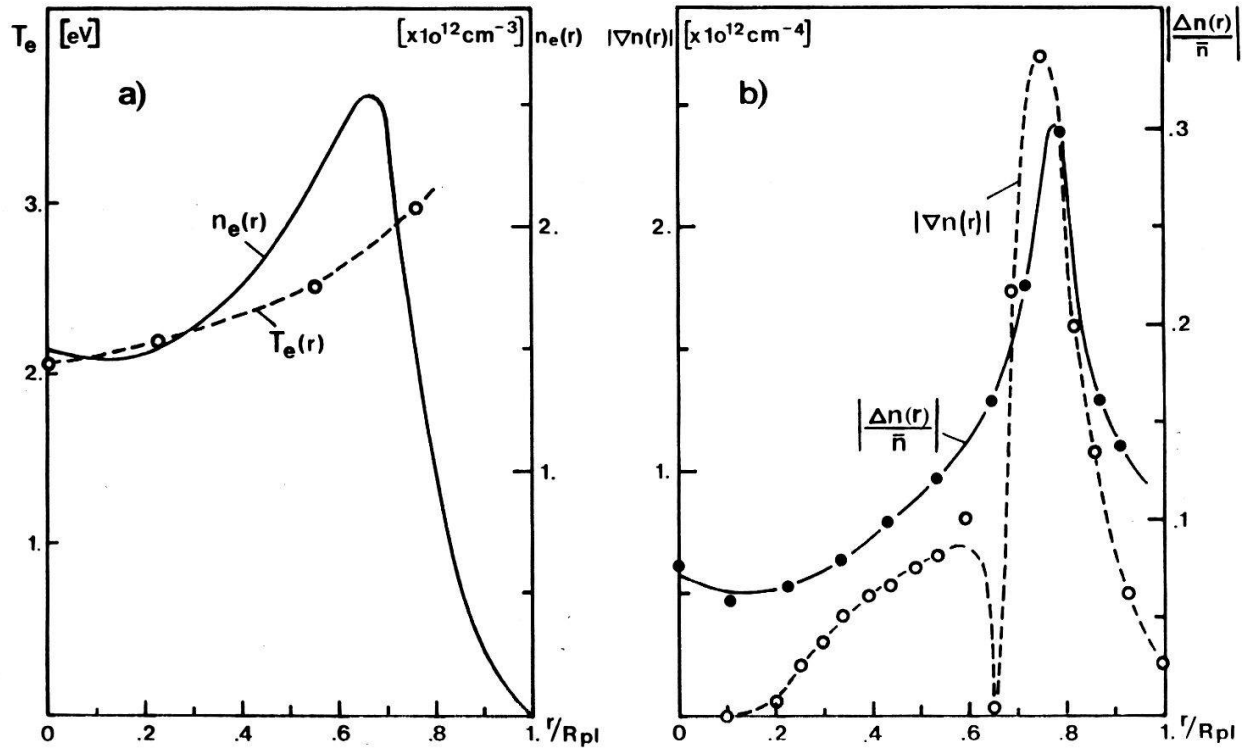

Figure 6
(a) Radial density and temperature profiles. (b) Total density fluctuations (coherent and random parts), where $\left|\frac{\Delta n}{\bar{n}}\right| = \frac{1}{\bar{n}}\left(\int_0^\infty n^2(\omega)\, d\omega\right)^{1/2}$, and density gradient determined from the density profile.

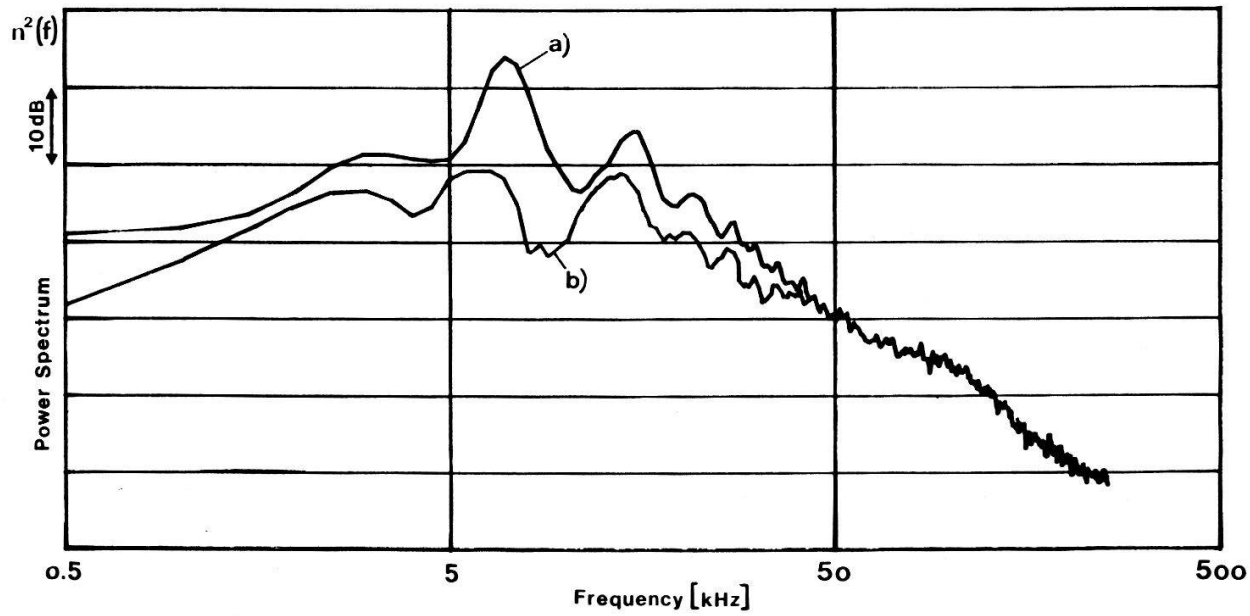

Figure 7
(a) Auto-power spectrum. The probe is positioned at maximal fluctuation ($r_{max}/R_{pl} = 0.75$). (b) The random power of the signal. This curve is estimated by subtracting the coherent power from the total power. The Nyquist-frequency is $f_{Nyq} = 250$ kHz.

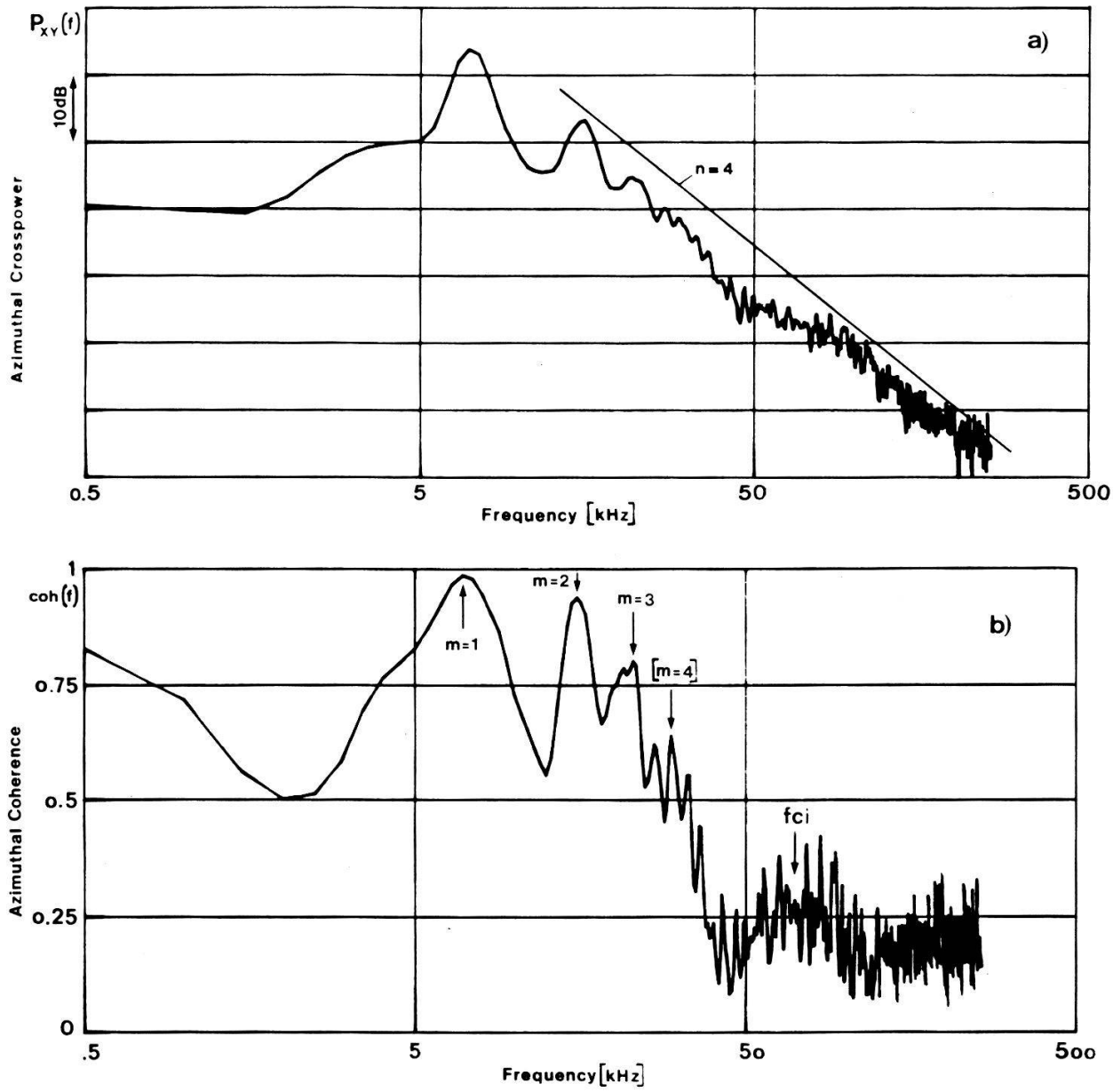

Figure 8
A typical set of spectra. Probe position $r_{max}/R_{pl} = 0.75$ and probe separation $\Delta\phi = 60°$, $\Delta r = \Delta z = 0$. cm. (a) The azimuthal cross-power spectrum for higher frequencies obeys the spectral index $n = 4$. (b) The coherence spectrum shows a high coherence for the $m = 1$ and $m = 2$ mode. The fluctuations at the minimum between these modes ($\simeq$11 kHz) are much more random. The estimate was evaluated over 25 data sets.

wave was found to be coherent for any probe separation parallel to $\mathbf{B}_0$ (Fig. 10c) and presents no phase shift. We thus conclude, that this mode is a standing wave in axial direction. Measurement of the amplitude of this spectral component as function of the axial position suggest a wave length λ_z of about twice the plasma length.

One type of instability which often occurs is called collisional drift instability, since it is tied to the diamagnetic drift of the electrons $\mathbf{v}_{De} = (cKT_e/eB_0^2 n)\, \nabla n \times \mathbf{B}_0$. The theories describing collisional drifts for fully as well as for weakly ionized plasmas are well known (e.g. [3–5, 38, 39]). Drift waves may appear as a result of the combined effects of density gradient, ion inertia and the electron motion

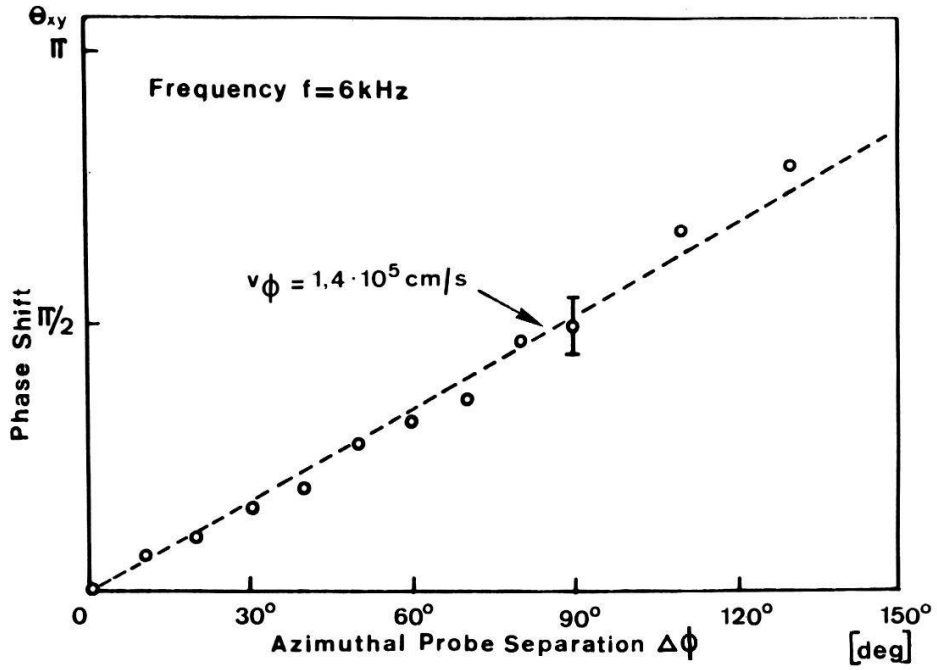

Figure 9
Phase shift between two probes as function of the azimuthal probe separation $\Delta\phi$, for the dominant first peak at 6 kHz. The dashed line represents the expected phase dependence for the $m = 1$ mode.

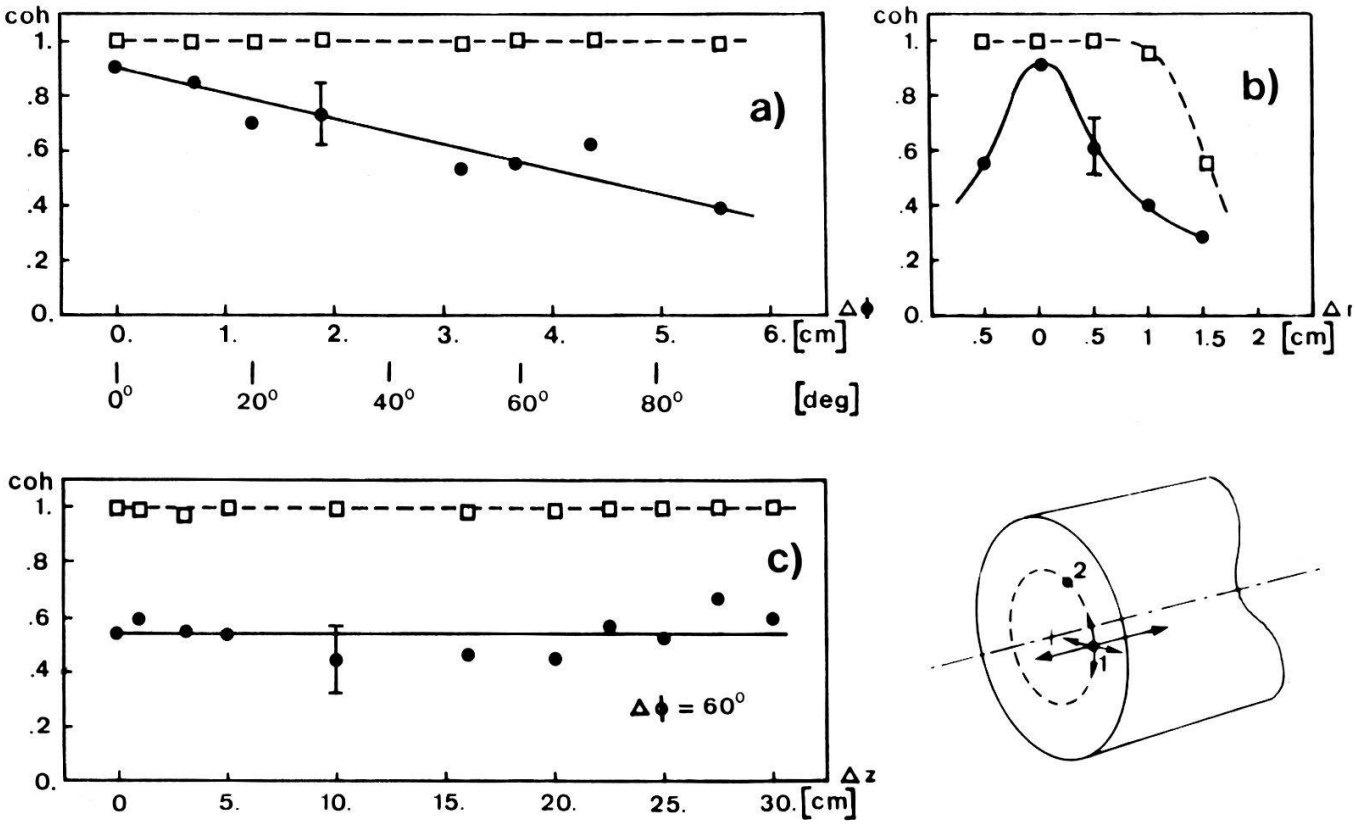

Figure 10
Coherence as a function of the probe separation (sketch) for a turbulent component (11 kHz) (—●—) and for the coherent wave at 6 kHz (—□—). One probe is always positioned at maximal fluctuation $r_{max} = 3.5$ cm. (a) Azimuthal dependence, (b) radial behaviour, (c) dependence in the z-direction. Here the probes are displaced azimuthally to prevent mutual interference.

parallel to the magnetic field. The driving mechanism for such instabilities results from the phase difference between the fluctuations of the electrostatic potential and the density. The phase difference is mainly caused by electron collisions.

We have estimated $\mathbf{v}_{De}$ on the basis of our plasma parameters. Assuming the maximum value of the density gradient from Fig. 6b we obtain $v_{De} = 3.1\ 10^5$ cm/s. The electron diamagnetic velocity is approximately twice as large as the measured phase velocity. Both velocities have the same direction. This factor of two is as predicted by the theory of Hendel and Chu [3] for maximal growth rate of collisional drift waves in highly ionized plasmas. Here we have neglected the Doppler shift resulting from the $\mathbf{E}_r \times \mathbf{B}_0$-rotation of the plasma, because the radial electric field is estimated to be weak ($\mathbf{E}_r \simeq (KT_i/e)(\nabla n/n)$, [40]).

The maximal growth rate of the unstable modes is theoretically predicted to occur at very large parallel wave lengths and is thus influenced by the finite plasma length. Schlitt and Hendel [39] have shown, that for the condition $L_{pl} \gg L_e$, the axial wave length is $\lambda_z \simeq 2L_{pl}$ and that the wave behaves as a standing wave in this direction. L_e is the mean free path of the electrons. In our plasma we find that the experiments are well consistent with $\lambda_z \simeq 2L_{pl}$ for the axial direction of the dominant wave.

Since the plasma is cylindrical, the azimuthal wave length λ_ϕ of the unstable modes is quantized by $\lambda_\phi \simeq 2r_{max} \cdot \pi/m$, whereby m represents the mode number of the form $\exp(im\phi)$. The dominant peak in the spectrum at 6 kHz can thus be identified as $m = 1$ mode.

Because the phase velocity and direction of wave propagation, as well as the wave length are consistent with the theoretical predictions, we conclude the wave at 6 kHz to be the $m = 1$ mode of collisional drift waves.

Should the magnetic field $\mathbf{B}_0$ be strong enough, then several modes may simultaneously become unstable. The further marked coherent peaks of the spectrum (Fig. 8(b)) are identified as harmonic drift waves ($m = 2, 3$ and even 4). Whether these peaks are self excited or decaying products can not be decided. For this, simulations based on a non local cylindrical model for arbitrary density profiles must be performed. Such calculations were made for weakly ionized plasmas by Ellis and Marden–Marshall [38], but are beyond the scope of the present work.

2. *Investigation of the turbulence and its anisotropy*

Beside the coherent drift instability the power spectrum (Fig. 7) shows a broad band of density fluctuations with decreasing power at higher frequencies. This fact will be investigated in detail.

The coherence spectrum (Fig. 8b) is characterized by two distinct regions. The transition between these domains does not depend on the azimuthal probe separation. The high frequency part, beyond about 40 kHz, always shows a very low coherence. Below this frequency the spectrum attains remarkably higher values and is dominated by a few strongly coherent peaks, discussed in IV.1.

The coherence for varying probe separations of a turbulent component and of the coherent mode $m = 1$ is represented in Fig. 10. The turbulence is measured at the minimum between the $m = 1$ and $m = 2$ mode, that is according to Fig. 6b

at 11 kHz. The self-excited wave is coherent throughout the entire region of strong density fluctuation. The turbulent eddies have on the contrary only a limited mean elongation in the plane perpendicular to the magnetic field. The radial coherence length l_r is smaller than that in the azimuthal direction l_ϕ ($l_r \simeq 0.7$ cm, $l_\phi \simeq 3.0$ cm). The coherence length in the axial direction l_z is of the order L_{pl} and is much longer than perpendicular to B_0. Thus the ratio of the coherence lengths is $l_r : l_\phi : l_z \simeq 0.7 : 3.0 : 100$. A similar result was recently found in a tokamak experiment by [41].

The dispersion relation $k_\phi(\omega)$ obtained from the phase spectrum (equation (24)) is practically linear (Fig. 10). The mean phase velocity ω/k_ϕ is thus constant over the frequency range up to 125 kHz and is close to the phase velocity measured for the $m=1$ mode of collisional drift waves. This suggests the interpretation of our observations as drift wave turbulence. In the following we shall compare these observations with an existing theory.

Comparision with theory. A theory dealing with the nonlinear behaviour and the turbulence spectrum of drift waves was developed by Hasegawa et al. [42, 17]. Although this theory is made for collisionless plasmas, the mechanism of the decay of the drift waves is not essentially different and it seems, that the theory is also applicable for our range of parameters [43].

These authors use a two dimensional model of the plasma ($k_z = 0$), i.e. the fluctuations in the z-direction are supposed to be infinitely extended. This assumption is consistent with our observation of constant coherence along the magnetic field lines. The decay is shown by these authors to occur as a result of three wave coupling, $\mathbf{k}_1 + \mathbf{k}_2 + \mathbf{k}_3 = 0$, $\omega_1 + \omega_2 + \omega_3 = \Delta\omega$, where $\Delta\omega$ is the frequency mismatch. As pump wave they considered a drift wave of given amplitude and they have simulated the decay of this mode numerically. The result is a power spectrum which exhibits two regions. The transition between these domains can be estimated from a characteristic wave number k_c, whereby k_c is defined according to [44, equation (21)]. For our plasma it follows that $k_c \cdot \rho_s \simeq 1$, where ρ_s represents the effective Larmor radius: $\rho_s = r_{ci} \cdot (T_e/T_i)^{1/2}$. The wave number k_c is thus for our parameters $k_c \simeq 1/\rho_S \simeq 2\ \mathrm{cm}^{-1}$. From the dispersion relation (Fig. 11) the corresponding frequency is given as $f_c(k_c) \simeq 50$ kHz. This frequency is about the same as found in our experiment for the transition between the two regions observed in the coherence spectrum (Fig. 8b).

For the domain of large wave numbers $k_\perp > k_c$ each mode is predicted by Hasegawa et al. to decay into a wave of longer and a wave of shorter wavelength whereby $\Delta\omega$ can admit values other than nought. The distribution of the power spectrum can be described by the spectral index n, whereby $P(\mathbf{k}) \propto k^{-n}$. The power spectrum, according to [17], decrease both in the radial and azimuthal direction with $n=4$. As a result, the turbulence is isotropic in $k_\perp$.

The measured weak coherence in this high frequency part of the spectrum may thus be explained by the fact, that the waves at a given frequency can couple with many different modes due to the allowed frequency mismatch. The contribution of each coupling product to the power is small and consequently also the coherence.

Since k_ϕ is a linear function of ω (Fig. 10) the fall off of the turbulent spectrum $P \propto k_\phi^{-n}$ predicted by the theory may be compared with the measured relationship $P \propto \omega^{-n}$. The slope of the azimuthal cross-power spectrum is in good

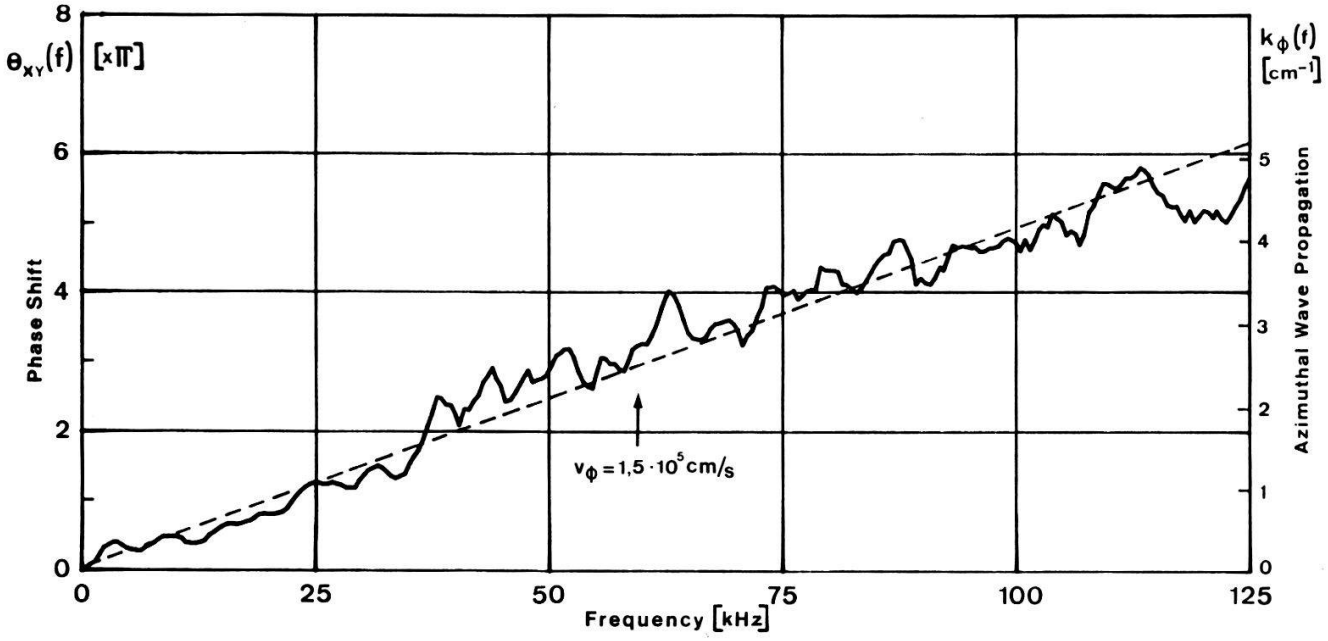

Figure 11
The dispersion relation $k_\phi(\omega)$ determined from the phase spectrum, corresponding to the cross-power spectrum of Fig. 9. $r_{max}/R_{pl} = 0.75$, $\Delta\phi = 60°$.

agreement with the predicted spectral index $n = 4$ (Fig. 8a). The small discrepancy around the ion cyclotron frequency shall not be discussed here.

For small wave numbers $k_\perp < k_c$, the theoretical model predicts the resonant three wave interaction with $\Delta\omega \simeq 0$ to be dominant. In the azimuthal direction the spectrum cascades to smaller wave numbers until $k_\phi = 0$. In the radial direction the power spectrum reaches its maximum when $k_r \simeq k_c$ and rapidly decreases for smaller wave numbers. The fluctuations are consequently anisotropic in this region of larger wave length in $k_\perp$.

In our experiment in fact this anisotropy has been found: At 11 kHz the ratio of the coherence length in radial direction to that in azimuthal direction is $l_r : l_\phi \simeq 0.7$ cm : 3.0 cm. This ratio is close to the expected anisotropy $1/k_r : 1/k_\phi =$ 0.5 cm : 2.0 cm. Here we assume that the power in r-direction condenses at k_c and thus that k_r at lower frequencies remains constant ($1/k_r \simeq 1/k_c = \rho_s \simeq 0.5$ cm). k_ϕ is found with the help of the measured dispersion relation.

Our observations are thus in agreement with the mentioned theory. However this comparision should not be extended to more details, because the theory works with one pump wave, whereas in our experiment we have evidently different unstable waves, acting as pump waves.

Bispectral analysis. With the help of the bispectrum it may be experimentally confirmed that the turbulent spectrum is generated by the unstable drift waves. Since the bispectrum has definite symmetrical properties [31] and the digital technique being limited by the Nyquist frequency, we may compute and plot the bicoherence spectrum (equation (27)) in the triangular region of the $f_1 f_2$-plane, defined by: $0 \leq f_2 \leq f_{Nyq}$, $f_1 \leq f_2$, $f_1 + f_2 \leq f_{Nyq}$.

Such a bicoherence spectrum is shown in Fig. 12. The dominant peak in this perspective view (a) indicates a relatively high phase coherence between $f_1 = f_{m=1} \simeq 6$ kHz, $f_2 = f_{m=2} \simeq 14$ kHz and $f_3 = (f_{m=1}, f_{m=2})$. We can conclude that the

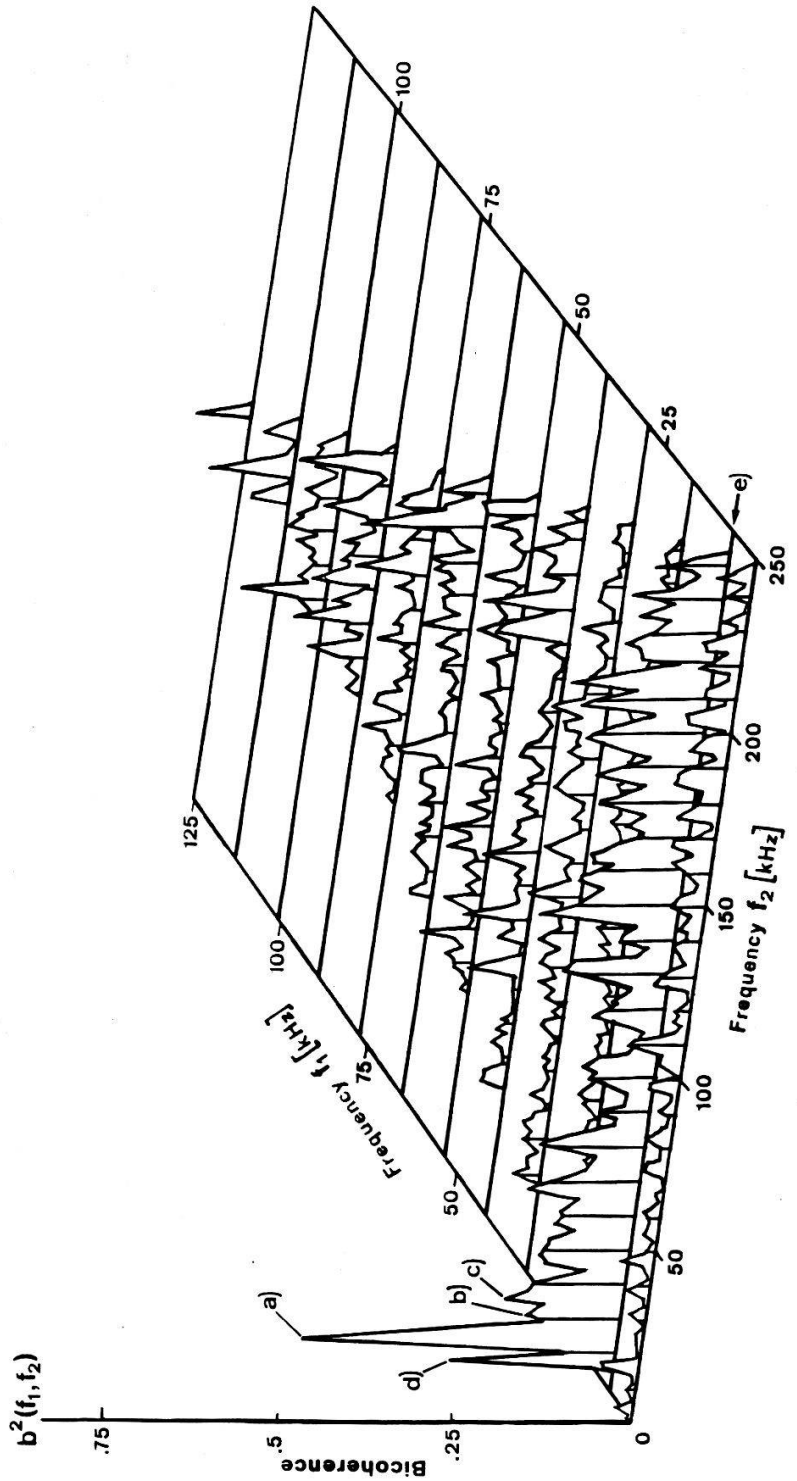

Figure 12
Perspective view of the bicoherence spectrum $b^2(f_1, f_2)$, estimated from 75 data sets. (a) Nonlinear interaction of the dominant drift waves $f_{m=1} \simeq 6$ kHz, $f_{m=2} \simeq 14$ kHz and $(f_{m=1}, f_{m=2}) = f_{m=1} + f_{m=2}$. (b) Interaction between $f_{m=1}, f_{m=3}$ and $(f_{m=1}, f_{m=3})$. (c) Three wave coupling between $m = 1$, $m = 4$ and the coupling product. (d) Harmonic generation of the $m = 1$ mode. (e) Bicoherence of the broad band spectrum f_2, the dominant $m = 1$ mode and the corresponding coupling products.

dominant instabilities interreact resonantly and generate a wave at their sum frequency $f_3 = f_{m=1} + f_{m=2} \simeq 20$ kHz. The decaying portion indeed appears in the coherence spectrum (Fig. 8b) as a peak somewhat below the frequency of the $m = 3$ mode. An eventual decay to lower frequencies was not found because the high-pass filter limits the experiment below 3 kHz. The interaction between $f_{m=1}$ and $f_{m=3}$ ($f_{m=4}$ resp.) is much weaker (Fig. 12(b), (c)). Beside the coupling of the strongly coherent and discrete modes, the bicoherences $b^2(f_1, f_2)$ of the $m = 1$ mode with the broad band spectrum f_2 and coupling components (f_1, f_2) are also noticeably enhanced compared to the remaining components (Fig. 12(e)).

Consequently we may conclude that there is a step-by-step development of the turbulent spectrum due to the interaction of the decaying portions, dominantly with the $m = 1$ and $m = 2$ modes. Except for the coupling with the coherent drift waves, the bicoherence spectrum remains small, as expected for components of a turbulent medium [6, p. 207] and as predicted by the theory for large wave numbers.

The random density fluctuations can thus be identified as turbulent drift waves, excited by mode coupling of unstable drift waves.

3. *Magnetoacoustic resonance*

As mentioned in the introduction, the investigation of the geometric resonances of a magnetized plasma cylinder presents a useful method to measure the electrical conductivity perpendicular to the magnetic field.

Since we use these experiments as a diagnostic tool, we concentrate on the first radial mode. We regard the cylinder as infinitely long. Experimentally it can be shown that in our case this is reasonable.

The magnetoacoustic resonance has been studied by many authors and is described theoretically as well as experimentally in detail in the literature (see for instance [8–14]). The theory will not be repeated here, but we must remember that the amplification in the resonance is described by the B_z field on the axis normalized to the B_z-component outside the plasma cylinder: $B_N = B(0)/B(R_{pl})$. Also the radial profie $B_N(r) = B(r)/B(R_{pl})$ can be calculated and measured. The amplification depends essentially on the electrical conductivity perpendicular to the magnetic field.

Many experiments, where the magnetoacoustic resonance has been measured in low density plasmas, show an amplification which can not be fitted by the theory, if a classical conductivity tensor is used [13–16, 45]. In these cases the plasma was not homogeneous and the amplification was much smaller than predicted by classical theory.

To demonstrate this we have measured the resonance in the experimental setup described in Section III. In Fig. 13 we see, that the classical theory gives an amplification of 20 (curve *c*), whereas the experiment shows an amplification of only 1.8. In Table 2 the frequencies, the amplification and the phase shift are given. The discrepancy between the experiment and the classical theory is evident.

To explain this descrepancy, some authors [45, 15, 16] have introduced 'effective collisions'. But these effective collisions are introduced ad hoc and there must be a physical interpretation. This interpretation is possible in terms of turbulence and we can use the conductivity tensor derived in Section II to describe our experiments. As we see from the results of the theory in Section II,

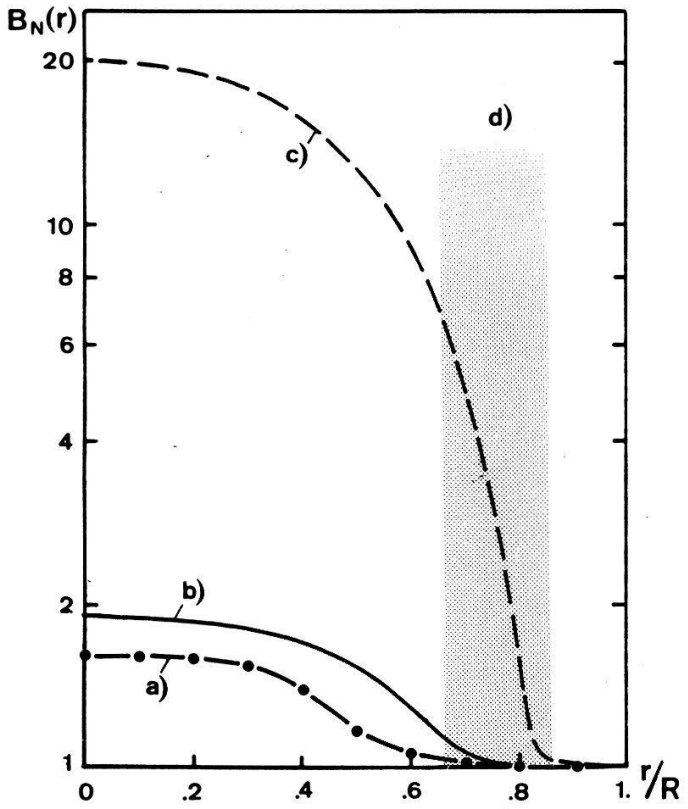

Figure 13
Radial dependence of B_N at the first magnetoacoustic resonance. (a) Experiment, (b) theory assuming the measured fluctuations, (c) theory excluding turbulence, (d) region of dominant turbulence.

we need for our calculation the amount of random density fluctuations $(\Delta n/\bar{n})^2(r)$ and the anisotropy.

The total fluctuations $(\Delta n/\bar{n})^2$ can be found by integrating the power spectrum over all frequencies. A result is shown in Fig. 6b. This value contains all fluctuations, the coherent self-excited drift waves and the stochastic turbulence. Since only the random fluctuation count for the damping an additional cross-power spectrum with large azimuthal probe separation ($\Delta s = 9$ cm $\hat{=} \Delta\phi = 120°$) gives us the amount contributed by the self-excited drift waves. For this we suppose the eddy size of the turbulence to be smaller than the probe separation. The radial

Table 2
Magnetoacoustic resonance, comparision between experiment and theory.

	f_0 [MHz]	$B_N = B(0)/B(R_{pl})$	$\Delta\varphi = \varphi(0) - \varphi(R_{pl})$ [$x\pi$]
argon			
experiment	4.	2.	0.2
theory without fluctuations	4.	20.	0.5
Theory with $\lvert\Delta n/\bar{n}\rvert_{max} = 11\%$ and $J = 30$	3.	1.9	0.25
helium			
experiment	12.5	2.8	0.4
theory with fluctuations	11.5	24.	0.5
Theory with $\lvert\Delta n/\bar{n}\rvert_{max} = 11\%$ and $J = 30$	9.	3.3	0.4

profile of the random fluctuations estimated in this way looks similar to Fig. 6.b, but the maximal fluctuations are reduced to $|\Delta n/\bar{n}| \simeq 11\%$.

The anisotropy factor $R(\theta, \varphi)$ of the turbulence, as defined by equation (14b), can not be measured directly, because we have not measured the k-spectrum of the eddies. In our experiment the anisotropy is measured in terms of coherence length in different directions $l_r : l_\phi : l_z \simeq 0.7 : 3 : 100$ and in this case there is a possibility to estimate the anisotropy factor. Since the anisotropy perpendicular to B_0 is small compared to that parallel to B_0 we assume no φ-dependence of the anisotropy factor. With this assumption, equation (19) leads to $J = 4 \cdot \pi \cdot R(\theta = \pi/2) \simeq l_z/l_\perp \simeq 30$.

With this value for $(\Delta n/\bar{n})^2(r)$ and the anisotropy factor J we are able to find $A_{x,y}$ of equation (17) and thus we can specify the conductivity tensor completely. This conductivity is considerably different to that one used in the classical theory for magnetoacoustic resonance. Here we have applied the numerical code written by E. Räuchle [46].

The results are plotted in Fig. 13 and 14. In Fig. 13 we see that the new conductivity tensor brings the amplification well into agreement with the experiment. The shaded area (d) marks the domain of dominant turbulence. We see that here the deviation with respect to the classical theory is most pronounced, because $A_{x,y}$ in equation (17) becomes very large. But this is in excellent agreement with the experimental observation. This strongly supports the idea that the turbulence is responsible for the damping of our resonance.

In Fig. 14 the amplification B_N and the phase shift $\Delta\varphi$ near the resonance are plotted. The theory shows the resonance at 3 MHz. The amplification is very near to that found in the experiment. At higher frequencies the agreement is not complete. The small peak at 10 MHz – the second magnetoacoustic resonance – appears in our experiment something more pronounced than in the theory. The

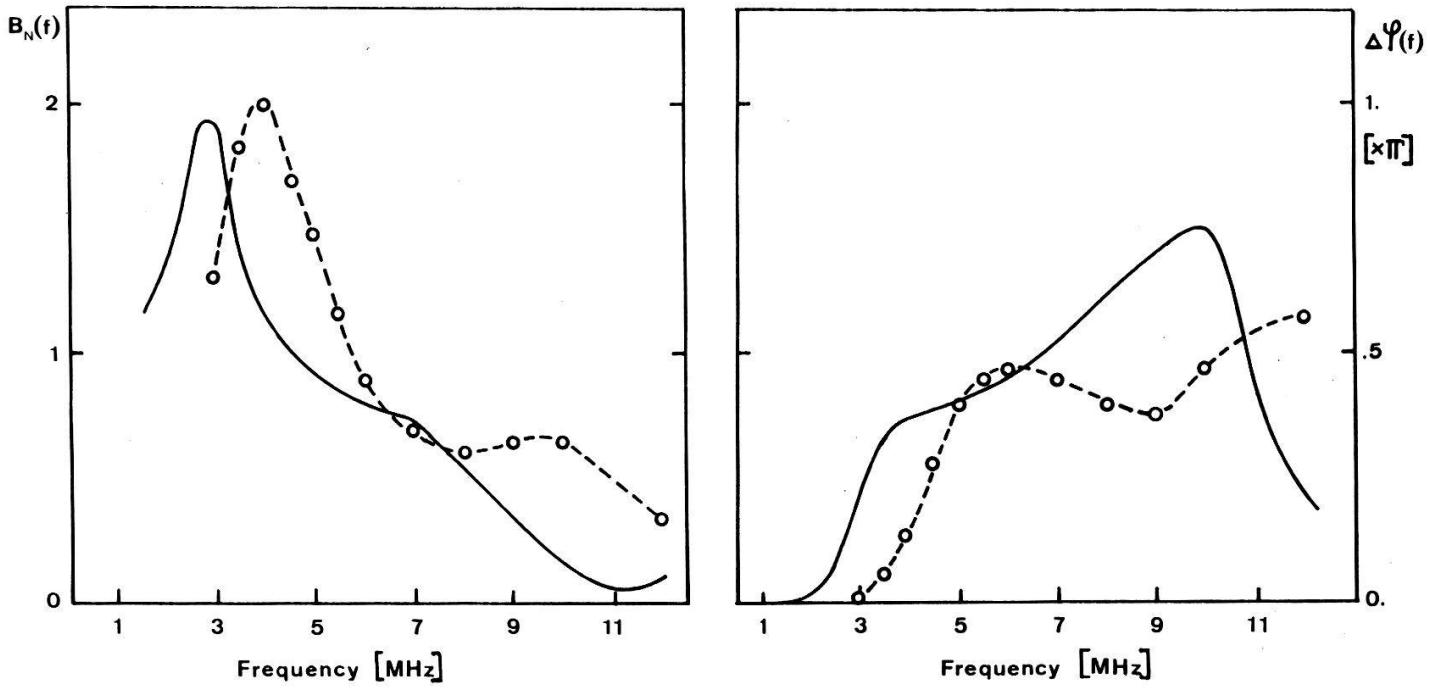

Figure 14
Normalized amplitude B_N and phase shift as function of the frequency in the region of the first magnetoacoustic resonance. Broken line: (--o--) experimental result; solid line (——) theoretical values.

small discrepancy in the resonance frequencies of experiment and theory may be due to the finite plasma length.

The same calculations were carried out for a helium plasma, published by Schneider et al. [15], and a hydrogen plasma, published by Krämer [13]. Both these plasmas have strong density gradients near the edge and all important parameters are given. So we can apply the criterion described by Timofeev and Shvilkin (Fig. 3 in [5]) and we find, that in both cases collisional drift instabilities must be expected similar to those described here. The results of the calculation for the helium plasma is given in Table 2. As we see the theory satisfactorily describes the amplification found in the experiment. For the case of hydrogen plasma [13] it seems that under similar assumptions about the density fluctuations it is possible to fit the data.

V. Summary and conclusion

We have presented in this paper the results of theoretical and experimental studies of the conductivity of a turbulent magnetoplasma for weak electromagnetic fields. The aim of this investigation is to find the influence of the turbulence on the electrical conductivity.

In a first step the dominant marked coherent instabilities appearing in the steep density gradient are identified as collisional drift waves ($m = 1, 2, 3$). The measured dispersion relation and distribution of the power spectrum leads us to identify the random density fluctuations as turbulent drift waves. The bicoherence spectrum shows that the turbulence is excited by mode coupling of the unstable drift waves.

The theoretical work is focused on a conductivity tensor including turbulent density fluctuations. The density variations are considered as time independent because of the much higher frequency of the r.f.-field. Further the target plasma is supposed not to be affected by the weak electromagnetic field. The theory shows that there is a substantially increased net electron current perpendicular to the static magnetic field. This current is controlled essentially by the random density fluctuations $(\Delta n/\bar{n})^2(r)$ and by the anisotropy of the turbulence.

The random density fluctuations and the anisotropy are measured.

The amplification of the magnetoacoustic resonance, which is very sensitive to the electrical conductivity of the plasma, is measured and compared with the results of the theory. The damping and radial wave field distribution of the resonance observed, in this article and by different authors, can be described by this theory in a straightforward manner provided the turbulence is known.

We conclude that the anomalous damping of the magnetoacoustic oscillations can be explained mainly by the influence of drift wave turbulence.

Acknowledgment

We would like to express our appreciation to Dr. E. Räuchle, University of Stuttgart, who kindly made a computer program available to us. We are also grateful to Dr. K. Appert, EPF-Lausanne, for valuable discussions.

REFERENCES

[1] D. BOHM, in: *The Characteristics of Electrical Discharges in Magnetic Fields* (Eds. A. Guthrie, R. K. Wakerling) McGraw-Hill, New York (1949).
[2] K. G. BUDDEN, J. of Research of the National Bureau of Standards *63D*, 135 (1959).
[3] H. W. HENDEL and T. K. CHU, in: *Plasma Physics Part A*, Academic Press (1970), p. 345.
[4] R. W. MOTLEY, in: *Q-Machines*, Academic Press, N.Y. (1975).
[5] A. V. TIMOFEEV and B. N. SHVILKIN, Sov. Phys. Usp. *19*, 149 (1976).
[6] B. KADOMTSEV, in: *Phénomènes collectifs dans les plasmas*, Editions MIR (Moscou 1979), p. 205.
[7] H. W. Hendel and T. K. Chu, Rep. MATT-730, Princeton Univ. Plasma Phys. Lab., Princeton (1969).
[8] M. H. BRENNAN, A. L. MCCARTHY and M. L. SAWLEY, Plasma Phys. *22*, 77 (1980).
[9] B. G. VAUCHER, J. VACLAVIK and H. SCHNEIDER, Helv. Phys. Acta *48*, 699 (1975).
[10] D. A. FRANK-KAMENETSKII, Soviet Phys. JETP *12*, 469 (1961).
[11] B. HOEGGER, K. APPERT, K. FÄSSLER, L. KRLIN and H. SCHNEIDER, Helv. Phys. Acta *44*, 321 (1971).
[12] H. P. ELMIGER, B. G. VAUCHER, H. SCHNEIDER and J. VACLAVIK, Plasma Phys. *20*, 921 (1978).
[13] M. KRÄMER, Plasma Phys. *17*, 373 (1975).
[14] B. LAMMERS, U. OBERLACK and H. SCHLÜTER, Z. Naturforsch. *30a*, 204 (1975).
[15] H. SCHNEIDER, B. A. HOEGGER, CH. RITZ, B. G. VAUCHER and T. M. TRAN, Helv. Phys. Acta *53*, 40 (1980).
[16] K. GROSSE and M. KRÄMER, Phys. Lett. *86A*, 152 (1981).
[17] A. HASEGAWA, C. G. MACLENNAN and Y. KODAMA, Phys. Fluids *22*, 2122 (1979).
[18] S. YOSHIKAWA and D. J. ROSE, Phys. Fluids *5*, 334 (1962).
[19] A. V. KADOMTSEV, in: *Plasma Turbulence*, Academic Press, New York (1965), p. 119.
[20] A. A. VEDENOV, in: *Theory of turbulent plasma*, Iliffe Books (1968), p. 49.
[21] Y. S. SAYASOV, Phys. Lett. *82A*, 337 (1981).
[22] T. HAAR, in: *Introduction to the Physics of Many-Body Systems*, Interscience Publ. Inc., New York (1958), Appendix B.
[23] N. A. KRALL and A. W. TRIVELPIECE, in: *Principles of Plasma Physics*, McGraw-Hill, Kogakusha (1973), p. 550.
[24] J. MUSIL and F. ZACEK, Plasma Phys. *16*, 735 (1975).
[25] B. A. HOEGGER, CH. RITZ, H. SCHNEIDER and B. G. VAUCHER, Phys. Lett. *84A*, 250 (1981).
[26] J. ROTH and W. M. KRAWCZONEK, Rev. Sci. Instr. *42*, 589 (1971).
[27] J. S. SERAFINI, Rep. NASA TM-X-1975, (1970).
[28] J. BENDAT and A. PIERSOL, in: *Random Data, Analysis and Measurement Procedures*, Wiley-Interscience, (1971).
[29] G. JENKINS and D. WATTS, in: *Spectral Analysis and its Application*, Holden-Day, San Francisco (1968).
[30] L. TICK, in: *Spectral analysis of time series*, Wiley, New York (1967), p. 133.
[31] Y. C. KIM and E. J. POWERS, IEEE Trans. Plasma Sci. *PS-7*, 120 (1979).
[32] K. G. SCHOENBERG, Rev. Sci. Instr. *51*, 1151 (1980).
[33] A. MONIN and A. M. YAGLOM, in: *Statistical Fluid Mechanics II*, MIT-Press, Massachusetts Institut of Techn. (1975).
[34] Y. C. KIM and E. J. POWERS, Phys. Fluids *21*, 1452 (1978).
[35] Y. C. KIM, J. M. BEALL, E. J. POWERS and R. W. MIKSAD, Phys. Fluids *23*, 258 (1980).
[36] R. B. BLACKMAN and J. W. TUKEY, in: *The Measurement of Power Spectra*, Dover, New York (1958).
[37] Y. C. KIM and E. J. POWERS, IEEE Trans. Plasma Sci. *PS-5*, 31 (1977).
[38] R. F. ELLIS, E. MARDEN-MARSHALL and R. MAJESKI, Plasma Phys. *22*, 113 (1980).
[39] L. G. SCHLITT and H. W. HENDEL, Phys. Fluids *15*, 1578 (1972).
[40] M. P. EVRARD, A. M. MESSIAEN, P. E. VANDENPLAS and G. VAN OOST, Plasma Phys. *21*, 999 (1979).
[41] S. J. ZWEBEN and R. J. TAYLOR, Nucl. Fusion *21*, 193 (1981).
[42] A. HASEGAWA and K. MIMA, Phys. Fluids *21*, 87 (1978).
[43] A. HASEGAWA, personal communication.
[44] H. OKUDA, T. SATO, A. HASEGAWA and R. PELLAT, Phys. Fluids *23*, 1965 (1980).
[45] B. A. HOEGGER, CH. RITZ, H. SCHNEIDER and B. G. VAUCHER, Phys. Lett. *76A*, 393 (1980).
[46] E. RÄUCHLE, Rep. IPF-72-8, Institut f. Plasmaforschung, Univ. Stuttgart.